Global Nuclear Fuel
A Joint Venture of GE, Toshiba, & Hitachi

Global Nuclear Fuel
Scott P. Murray
Manager, Licensing & Liabilities

3901 Castle Hayne Road
P.O. Box 780
Wilmington, NC 28402
USA

(910) 819-5950
(910) 362-5950
Scott.murray@ge.com

SPM 11-030

July 27 2011

Ms. Kimberly Hardin
Licensing Branch – Division of Spent Fuel Storage and Transportation
Office of Nuclear Material Safety and Safeguards
U.S. Nuclear Regulatory Commission
Washington, DC 20555-0001

ATTN: Document Control Desk

Dear Ms. Hardin:

Subject: GNF-A Response to NRC Request for Additional Information Dated 12/23/10 for Model No. RAJ-II Package

References:
1) Docket Number 71-9309
2) GNF-A Request for Revision to the Certificate of Compliance No. 9309 for the RAJ-II Transportation Package, 7/13/10
3) NRC Request for Additional Information, H Akhavannik to S. P. Murray, 12/23/10
4) GNF-A letter Requesting Response Extension, S. P. Murray to H. Akhavannik, 1/28/11
5) GNF-A letter Requesting Response Extension, S. P. Murray to H. Akhavannik, 6/30/11

Attached is Global Nuclear Fuel - Americas, LLC (GNF-A) response to NRC's request for additional information (RAI) dated December 23, 2010 (Reference 3). We appreciate the NRC Staff's ongoing review of this request.

Please note, a separate letter will be submitted containing Westinghouse Electric Corporation company proprietary information in support of these RAI responses.

Please contact me on (910) 819-5950 if you have any questions or would like to discuss this matter further.

Sincerely,

Scott P. Murray, Manager
Licensing & Liabilities

Commitments: None

Attachment : GNF-A RAI response

NMSS26

NRC RAI for RAJ-II Package – Docket No. 71-9309, TAC No. L24456:

Editorial Requests:

2.0 Structural

2-1 Provide an additional hardcopy of the input and output structural modeling files for LTP, Cladding, and Impact Analysis, previously submitted in the September 27, 2010 submittal. This information is required in order to provide a complete submittal of the September 27, 2010, supplemental information to the Document Control Desk to have the record updated.

Response:

Input and output files for the LS-DYNA and ANSYS analyses presented in the September 27, 2010 have been transmitted to the NRC. Additionally, the input and output files for the analyses performed to address these RAI's will be transmitted to the NRC following the receipt of this letter report.

2-2 Please correct the figures on pp 2-104 and 2-105 as the content of the graphs is missing. This information is needed to determine compliance with 10 CFR 71.73.

Response:

The corrected figures were previously transmitted to the NRC. The corrected figures will be included in the latest SAR revision.

7.0 Package Operation

7-1 Fix the numbering in Chapter 7.1.2.1, "Outer Container Lid Removal," to have the numbering begin with the number "1" instead of the number "6." This information is required in order for the staff to ensure that the application will meet the requirements of 1 0 CFR 71.33.

Response:

The corrected numbering will be included in the latest SAR revision.

NRC RAI for RAJ-II Package – Docket No. 71-9309, TAC No. L24456:

Structural Questions:

2-1 Provide labels for tables and figures in Section 2.12.5.

Response:

Section 2.12.5 of the RAJ-II will be revised to provide labels for tables and figures. The list of figures and tables will also be updated.

NRC RAI for RAJ-II Package – Docket No. 71-9309, TAC No. L24456:

2-2 Revise plot on p 2-92. Plot of Total True Stress versus Plastic True Strain is plotted incorrectly or labeled incorrectly. The values shown in the plot are Total Engineering Stress versus Total Engineering Strain.

Response:

Plot on p 2-92 corrected as follows:

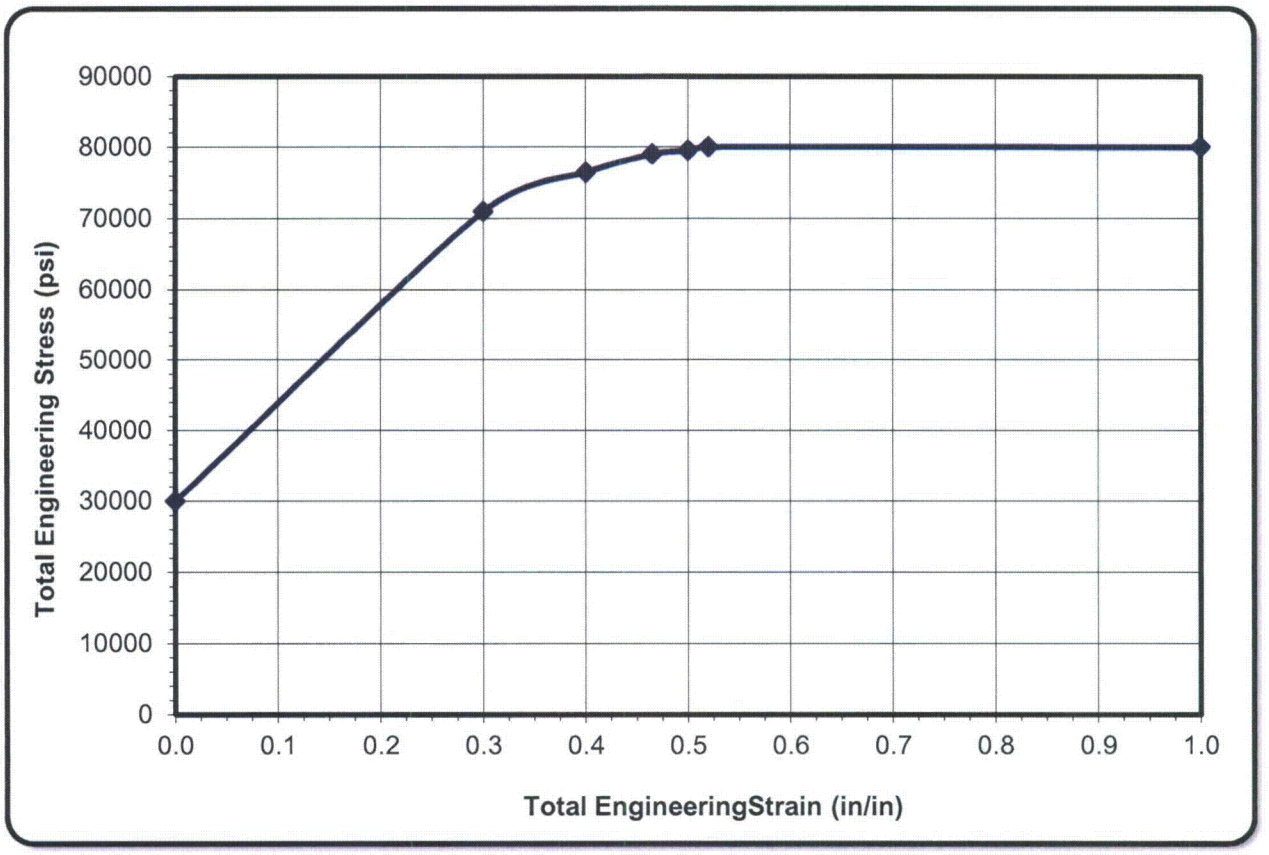

NRC RAI for RAJ-II Package – Docket No. 71-9309, TAC No. L24456:

2-3 Provide additional tabular data for shear stress as defined by Load Curve 1006 for paper honeycomb material properties (pp 2-92, 2-93). Reported material properties are for normal stress alone in the corresponding table.

Response:

The paper honeycomb material properties used in the LS-DYNA drop analyses are presented below. Both normal and shear stress-volumetric strain data is provided. The properties are based on laboratory test data and crush data recorded following the drop test. Further discussion is presented in the responses to RAIs 2-10 and 2-13.

```
*MAT_HONEYCOMB_TITLE
Honeycomb
$#     mid        ro         e        pr      sigy        vf        mu      bulk
         7 1.5000E-5  19.59E+6     0.450 1.0000E+6   .050000  0.050000  1.000000
$#     lca       lcb       lcc       lcs      lcab      lcbc      lcca      lcsr
      1003      1003      1003      1006      1006      1006      1006
$#    eaau      ebbu      eccu      gabu      gbcu      gcau      aopt      macf
  53550.00  53550.00  53550.00  35437.00  35437.00  35437.00  2.000000
$#      xp        yp        zp        a1        a2        a3
  1.000000     0.000     0.000  1.000000
$#      d1        d2        d3      tsef      ssef
     0.000  1.000000

*DEFINE_CURVE
$#    lcid      sidr       sfa       sfo      offa      offo    dattyp          Honeycomb
      1003         0     0.000   0.23600     0.000     0.000         0
$#                a1                  o1
0.140,   201
0.200,   201
0.247,   198
0.341,   191
0.435,   169
0.529,   130
0.624,   104
0.718,   77
0.812,   59
0.906,   55
1.000,   40
1.100,   40

*DEFINE_CURVE
$#    lcid      sidr       sfa       sfo      offa      offo    dattyp          Honeycomb
      1006         0     0.000   0.23600     0.000     0.000         0
$#                a1                  o1
0.140,   101
0.200,   101
0.247,   100
0.341,   99
0.435,   96
0.529,   85
0.624,   65
0.718,   52
0.812,   39
0.906,   30
1.000,   28
1.100,   28
```

NRC RAI for RAJ-II Package – Docket No. 71-9309, TAC No. L24456:

2-4 Revise or clarify paper honeycomb stress strain curves. The paper honeycomb stress strain curves (p 2-93) are representative of stress versus strain rather than stress versus volumetric strain, which is the required input parameter for LS-DYNA.

Response:

The following is the stress versus relative volume properties used in the LS-DYNA model. The stress-strain curves on p 2-93 of the SAR will be revised to present these properties. Refer to the responses to RAIs 2-10 and 2-13 for details how the properties were verified.

Stress-Strain Properties for Paper Honeycomb

Relative Volume	Stress (psi) at 21°C	Stress (psi) at 77°C	Stress (psi) at -40°C
0.140	152	201	215
0.200	152	201	215
0.247	145	198	198
0.341	140	191	197
0.435	132	169	173
0.529	122	130	154
0.624	109	104	153
0.718	98	77	144
0.812	84	59	120
0.906	77	55	77
1.000	67	40	62
1.100	67	40	62

NRC RAI for RAJ-II Package – Docket No. 71-9309, TAC No. L24456:

2-5 Revise or clarify the stress strain table for Ethafoam. The stress strain table on p 2-94 for Ethafoam has the same values as the paper honeycomb in the table on p 2-93 and staff is unclear whether this is an accurate representation.

Response:

The following table is the stress-strain properties for Ethafoam as determined by laboratory testing. The strain values were corrected to reflect the LS-DYNA input, i.e. Load Curve 1005. The applicant will ensure the proper properties are identified in the SAR text and in response to RAI 2-1 sequentially numbered.

Stress-Strain Properties for Ethafoam

Volumetric Strain	Stress (psi) at 21°C	Stress (psi) at 77°C	Stress (psi) at -40°C
0.000	0	0	0
0.014	9	3	11
0.028	12	5	15
0.042	13	7	17
0.056	15	9	19
0.071	18	11	23
0.085	23	15	27
0.099	29	20	35
0.113	41	28	47
0.127	63	42	70
0.134	84	55	91

NRC RAI for RAJ-II Package – Docket No. 71-9309, TAC No. L24456:

2-6 Revise or clarify the stress strain table for Ethafoam or revise Load Curve 1005. The values input for Load Curve 1005 for *MAT_CRUSHABLE_FOAM do not match the values presented in the table on p 2-94 for Ethafoam.

Response:

The corrected table for Ethafoam is provided in the response for RAI 2-5. The values for the table now reflect the LS-DYNA input for Load Curve 1005. The following are the Load Curve 1005 values at the three temperature conditions considered.

Stress (psi) at 21°C

```
*DEFINE_CURVE
$#     lcid      sidr       sfa       sfo      offa      offo     dattyp
       1005
$              STRAIN           STRESS
$#                 a1                o1
                0.000             0.000
            0.0140000         9.0000000
            0.0280000        12.0000000
            0.0420000        13.0000000
            0.0560000        15.0000000
            0.0710000        18.0000000
            0.0850000        23.0000000
            0.0990000        29.0000000
            0.1130000        41.0000000
            0.1270000        63.0000000
            0.1340000        84.0000000
```

Stress (psi) at 77°C

```
*DEFINE_CURVE
$#     lcid      sidr       sfa       sfo      offa      offo     dattyp
       1005
$              STRAIN           STRESS
$#                 a1                o1
                0.000             0.000
            0.0140000         3.0000000
            0.0280000         5.0000000
            0.0420000         7.0000000
            0.0560000         9.0000000
            0.0710000        11.0000000
            0.0850000        15.0000000
            0.0990000        20.0000000
            0.1130000        28.0000000
            0.1270000        42.0000000
            0.1340000        55.0000000
```

Stress (psi) at -40°C

```
*DEFINE_CURVE
$#     lcid      sidr       sfa       sfo      offa      offo     dattyp
       1005
$              STRAIN           STRESS
$#                 a1                o1
                0.000             0.000
            0.0140000        11.0000000
            0.0280000        15.0000000
```

0.0420000	17.0000000
0.0560000	19.0000000
0.0710000	23.0000000
0.0850000	27.0000000
0.0990000	35.0000000
0.1130000	47.0000000
0.1270000	70.0000000
0.1340000	91.0000000

NRC RAI for RAJ-II Package – Docket No. 71-9309, TAC No. L24456:

2-7 Clarify the strain input values shown on p 2-95. Staff is unclear if the strain input values labeled Plastic True Strain shown in the table are equivalent to volumetric strain.

Response:

A complete review of the material properties was performed, and the properties for the aluminum silicate insulation (Duraboard), hemlock and balsa wood were updated since the last submittal to the NRC. Therefore, the material properties presented on p 2-95 will be updated with the data provided in this RAI response. Like the Ethafoam curves on p 2-94, the crushable materials will be presented in the SAR as stress-strain. The simple model presented in the response to RAI 2-13 was used to verify the LS-DYNA input.

The properties for the aluminum silicate insulation are derived from the manufacturer's data sheet and accounts for the behavior of the material when compress to a solid height while air is pressed out of the fabric/ceramic layers. The crushable foam material model is used for stability. The aluminum silicate provides little energy absorption but is modeled as accurately as possible.

```
*DEFINE_CURVE
*MAT_CRUSHABLE_FOAM_TITLE
Insulation
$#     mid        ro         e        pr      lcid       tsc      damp
         8 1.5000E-5 1.2500E+5  0.400000      1004     0.000  0.500000

*DEFINE_CURVE
$#    lcid      sidr       sfa       sfo      offa      offo    dattyp          Duraboard
      1004         0     0.000     0.000     0.000     0.000         0
$#                a1                  o1
0.00,    0
0.05,    42
0.10,    50
0.15,    57
0.30,    300
0.50,    1000
0.70,    100000
0.90,    500000
```

Hemlock is used as a non-conductive separator between the inner container and outer shell layers that provides no impact protection. The properties for Hemlock are similar to Douglas-fir, pine and balsa wood and are derived from information available in open literature. Because of negative volume issues, a smooth curve with positive slope was derived. The following properties were used in the LS-DYNA analyses.

```
*MAT_CRUSHABLE_FOAM_TITLE
```

```
Hemlock
$#     mid        ro         e        pr      lcid       tsc      damp
         3 1.5000E-5 1.2500E+5  0.400000      1001     0.000  0.100000

*DEFINE_CURVE
$#    lcid      sidr       sfa       sfo      offa      offo    dattyp          Hemlock
      1001         0     0.000     0.000     0.000     0.000         0
$#                a1                  o1
               0.000               0.000
           0.0100000        1250.0000000
           0.0950000        2537.0000000
           0.1820000        2638.0000000
           0.2620000        2937.0000000
           0.3360000        3249.0000000
           0.5300000        3946.0000000
           0.6930000        4642.0000000
```

For the balsa properties, the hemlock properties were used as a starting point and expanded based on the known crush response experienced during the end drop. The modified crushable foam model was used to allow for strain rate effects.

```
*MAT_MODIFIED_CRUSHABLE_FOAM_TITLE
Balsa Perpendicular - Ambient temperature
$#     mid        ro         e        pr       tid       tsc      damp    ncycle
       302 1.2000E-5 66500.000     0.000      3200     0.000  0.150000 100.00000
$#  srclmt    srflag
     0.000         0
$---+----1----+----2----+----3----+----4----+----5----+----6----+----7----+----8
*DEFINE_TABLE
$ Balsa Perpendicular to grain - Ambient temperature
$ static
$#    tbid
      3200
$#             value      lcid
               0.000      3201
          25.0000000      3202
          75.0000000      3203
         375.0000000      3204
*DEFINE_CURVE
$#    lcid      sidr       sfa       sfo      offa      offo    dattyp
      3201         0     0.000  1.100000     0.000     0.000         0
$#                a1                  o1
               0.000               0.000
           0.0100000         665.0000000
           0.0250000        1065.0000000
           0.0500000        1265.0000000
           0.0750000        1365.0000000
           0.1000000        1405.0000000
           0.1250000        1445.0000000
           0.1500000        1485.0000000
           0.1750000        1520.0000000
           0.2000000        1555.0000000
           0.2250000        1590.0000000
           0.2500000        1625.0000000
           0.2750000        1660.0000000
           0.3000000        1695.0000000
           0.3250000        1730.0000000
           0.3500000        1765.0000000
           0.3750000        1800.0000000
           0.4000000        1835.0000000
           0.4250000        1870.0000000
           0.4500000        1905.0000000
           0.4750000        1940.0000000
           0.5000000        1980.0000000
           0.5250000        2020.0000000
           0.5500000        2080.0000000
           0.5750000        2160.0000000
```

```
          0.6000000        2260.0000000
          0.6250000        2460.0000000
          0.6500000        2860.0000000
          0.6750000        3460.0000000
          0.7000000        4260.0000000
*DEFINE_CURVE
$#     lcid      sidr       sfa       sfo      offa      offo    dattyp
      3202         0     0.000  1.100000     0.000     0.000         0
$#               a1                    o1
             0.000                 0.000
          0.0100000         753.0000000
          0.0250000        1153.0000000
          0.0500000        1353.0000000
          0.0750000        1453.0000000
          0.1000000        1493.0000000
          0.1250000        1533.0000000
          0.1500000        1573.0000000
          0.1750000        1608.0000000
          0.2000000        1643.0000000
          0.2250000        1678.0000000
          0.2500000        1713.0000000
          0.2750000        1748.0000000
          0.3000000        1783.0000000
          0.3250000        1818.0000000
          0.3500000        1853.0000000
          0.3750000        1888.0000000
          0.4000000        1923.0000000
          0.4250000        1958.0000000
          0.4500000        1993.0000000
          0.4750000        2028.0000000
          0.5000000        2068.0000000
          0.5250000        2108.0000000
          0.5500000        2168.0000000
          0.5750000        2248.0000000
          0.6000000        2348.0000000
          0.6250000        2548.0000000
          0.6500000        2948.0000000
          0.6750000        3548.0000000
          0.7000000        4348.0000000
*DEFINE_CURVE
$#     lcid      sidr       sfa       sfo      offa      offo    dattyp
      3203         0     0.000  1.100000     0.000     0.000         0
$#               a1                    o1
             0.000                 0.000
          0.0100000         766.0000000
          0.0250000        1166.0000000
          0.0500000        1366.0000000
          0.0750000        1466.0000000
          0.1000000        1506.0000000
          0.1250000        1546.0000000
          0.1500000        1586.0000000
          0.1750000        1621.0000000
          0.2000000        1656.0000000
          0.2250000        1691.0000000
          0.2500000        1726.0000000
          0.2750000        1761.0000000
          0.3000000        1796.0000000
          0.3250000        1831.0000000
          0.3500000        1866.0000000
          0.3750000        1901.0000000
          0.4000000        1936.0000000
          0.4250000        1971.0000000
          0.4500000        2006.0000000
          0.4750000        2041.0000000
          0.5000000        2081.0000000
          0.5250000        2121.0000000
          0.5500000        2181.0000000
          0.5750000        2261.0000000
          0.6000000        2361.0000000
          0.6250000        2561.0000000
```

```
          0.6500000        2961.0000000
          0.6750000        3561.0000000
          0.7000000        4361.0000000
*DEFINE_CURVE
$#     lcid      sidr       sfa       sfo      offa      offo    dattyp
      3204         0     0.000  1.100000     0.000     0.000         0
$#               a1                    o1
           0.000                  0.000
          0.0100000         526.0000000
          0.0250000         926.0000000
          0.0500000        1126.0000000
          0.0750000        1226.0000000
          0.1000000        1266.0000000
          0.1250000        1306.0000000
          0.1500000        1346.0000000
          0.1750000        1381.0000000
          0.2000000        1416.0000000
          0.2250000        1451.0000000
          0.2500000        1486.0000000
          0.2750000        1521.0000000
          0.3000000        1556.0000000
          0.3250000        1591.0000000
          0.3500000        1626.0000000
          0.3750000        1661.0000000
          0.4000000        1696.0000000
          0.4250000        1731.0000000
          0.4500000        1766.0000000
          0.4750000        1801.0000000
          0.5000000        1841.0000000
          0.5250000        1881.0000000
          0.5500000        1941.0000000
          0.5750000        2021.0000000
          0.6000000        2121.0000000
          0.6250000        2321.0000000
          0.6500000        2721.0000000
          0.6750000        3321.0000000
          0.7000000        4121.0000000
```

NRC RAI for RAJ-II Package – Docket No. 71-9309, TAC No. L24456:

2-8 Provide acceleration time history for lower tie plate indicating a peak G load of 75 G's is conservative. This information is necessary to determine if appropriate loading or deformation for the fuel rods is consistent with that seen in the tests.

Response:

The 75G limit is chosen as a conservative value to bound the known measured peak acceleration. The RAJ-II Japanese SAR (USA/0495/AF-96) presents the following acceleration summary for the lower and upper tie plate accelerations during the 9 meter vertical drop:

"Because the acceleration sensors on the upper plate and the lower plate were separated from their binded places (mounts) measurement (at about 18 ms and at about 8ms after the drop), data are available only for those periods. In those periods, the peak exists as, 53g at 13 ms after the drop, and 58g at about 5ms."

To summarize, because the accelerometers broke from their mounts, a complete acceleration time-history trace is not available. However, a peak acceleration of 58G's is recorded at the lower tie plate. The value of 58G's is documented in Table 2-13 of the SAR.

Further analysis of the lower tie plate and fuel rods is provided in the response to RAI 2-9.

NRC RAI for RAJ-II Package – Docket No. 71-9309, TAC No. L24456:

2-9 Provide dynamic analysis of lower tie plate and fuel rod. A static analysis of fuel performance is not adequate to capture the potential damage from dynamic effects. The rigid body peak deceleration for packaging, whether from test or analysis, has been shown to be deficient when considering loading to the payload.

Response:

Lower Tie Plate Analysis

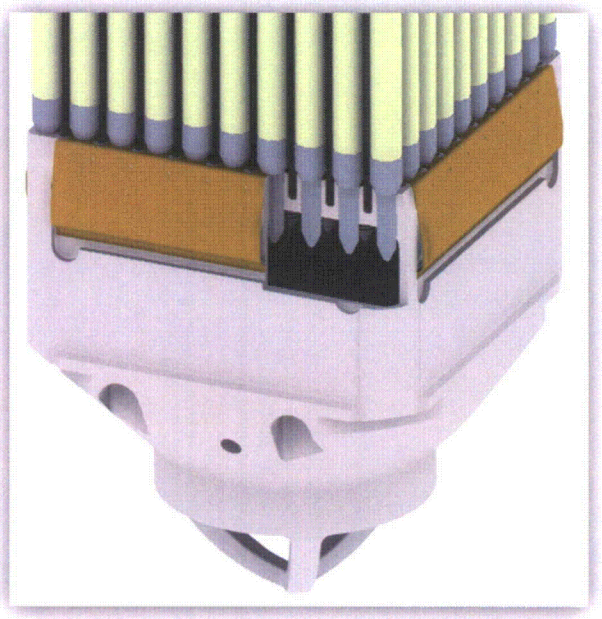

The lower tie plate (LTP) analysis was prepared to demonstrate to the French IRSN the geometry of the lower tie plate following the end drop. The IRSN was concerned about the performance of the LTP and the fuel rods interaction with the LTP. Unlike the standard PWR design, the fuel rods engaged into the BWR LTP.

Additionally, the analysis was used to show the post impact concave shape of the lower tie plate. This shape was important in addressing the post accident criticality limit. Analyses in Chapter 6 of the SAR showed that the reactivity of the bundle was reduced, because the fuel rods tended to form a tight grouping towards the center line of the bundle as the rods bowed inward.

To address this RAI, the ANSYS model of the LTP previously presented was ported to LS-DYNA to perform a fully dynamic analysis. Mass elements were used to represent the load applied to the lower tie plate by the fuel rods, water rods and tie rods. An instantaneous acceleration was applied to the model, and the run termination time was set based on the measured drop duration during the drop test. Two cases were identified that would impose an axial load on the LTP. As Table 2-9.1 shows, the measured acceleration was 58G during the end drop. However, the CG over corner evaluation produced higher accelerations at the LTP and inner container shell.

Table 2-9.1. End Drop and Corner Drop Test Acceleration Summary

Package	Test Location	Drop Orientation	Impact Duration (ms)	Acceleration (G)	Sensor Location
RAJ-II	Japan	Vertical end drop	30	58	Lower tie plate
RAJ-II	Japan	Vertical CG over corner	30	135	Lower tie plate
RAJ-II	Japan	Vertical CG over corner	30	203	Lower tie plate

For this evaluation, the CG over corner case was considered with a maximum acceleration of 203G. The impact load was applied to the model for 70 ms then returned to 1G loading conditions for 30ms. The resulting displacement calculated by LS-DYNA was 0.035 inches. Additional analyses were performed to determine the effect of time. It was noted that the displacement equivalent to the previous static analysis occurred at a time of approximately 0.5 seconds. Therefore, the static analysis bounded the dynamic analysis results.

Fuel Rod Cladding Analysis

In addition to the NRC RAI, the French IRSN had additional questions concerning the cladding analysis. Following are the additional questions and subsequent responses:

GNF analysis of the rod cladding resistance in HAC fire conditions is based on a three step analysis. First a deflection is applied to the rod to simulate external load applied by the tie plate; then this deflection is released; and finally the temperature is increased to simulate the fire conditions.

IRSN Questions:

1. *In the second step of the analysis, GNF releases the deflection to calculate the residual stress in the cladding. Wouldn't it be more penalizing to keep the rod deflected when applying the thermal stress?*
2. *Which is the elongation at rupture at high temperature for the cladding material considered in the analysis at high temperature?*
3. *Previous testing showed that an azimuthal temperature gradient can reduce the elongation at rupture of the cladding material. This should be taken into account in GNF analysis?*

Response to IRSN Questions:

Based upon the dynamic analysis of the LTP, the total deformation is measured at 0.035 inches which is equivalent to a deflection of about 1°. To bound the problem using ANSYS, a remote

displacement of 3° is applied during the first load step and maintained during the fire analysis. Therefore, stresses resulting from the mechanical loads are combined with the accident pressure stresses at fire accident temperatures. The analysis results show that during all cases the stresses are less than the ultimate strength of the material. Therefore, failure of the cladding is not expected which confirms the drop test results.

To address the second question, the material model includes the coefficient of thermal expansion and the model is fixed at the cladding free end. Therefore, thermal stresses are accounted for from the initial ambient condition through the fire. The combined stress at the end plug of the fuel cladding is shown below.

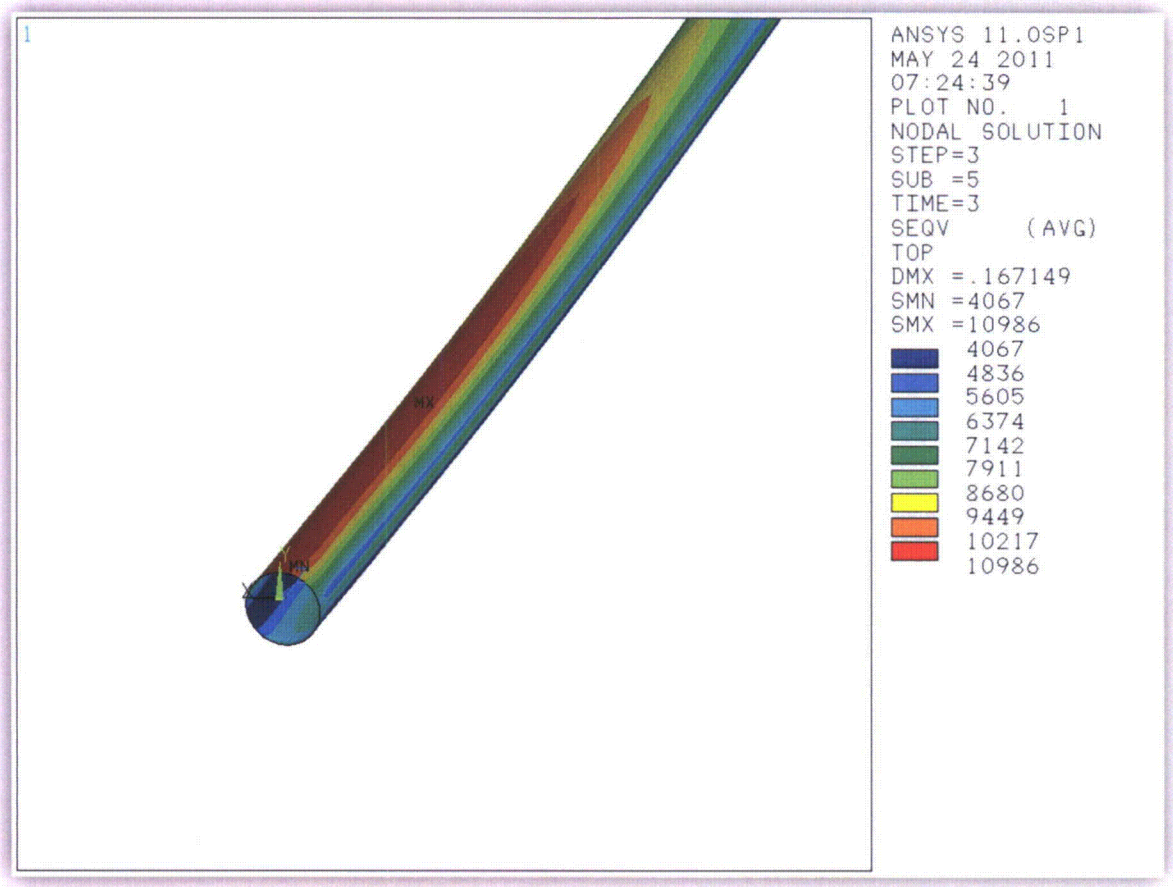

Figure 2-9.1. Combined Stress in Cladding During Load Step 3

Improved bi-linear material properties are used to evaluate the stresses in the cladding. At 648°C the yield stress is 11,854 psi, and the ultimate stress is 13,000 psi. Based on the stress analysis results, the conclusion from the original analysis still holds. During impact local yielding of the

cladding occurs then is stress relieved when the cladding temperature is raised from ambient conditions to the fire temperature. Therefore, rupture of the cladding does not occur.

In response to question 3, heating of the fuel cladding occurs along the axis of the fuel cladding during the fire, not around the circumference. For this analysis, thermal stresses occur along the length of the rod with no azimuthal variation from 21°C to 648°C, as such fuel azimuthal variations are not present in the stress distribution.

NRC RAI for RAJ-II Package – Docket No. 71-9309, TAC No. L24456:

2-10 Provide damage comparisons (displacements, stresses, etc.) with FEA models and CTUs. Simple comparison of peak decelerations is not sufficient when attempting to simulate test results with an analytical model.

Response:

For the side impact case involving the crushing of honeycomb, benchmarking of the results was accomplished by comparing the measured crush values of the honeycomb post drop test with a series of honeycomb nodal displacements along the length of the lid. The average post impact height values for both the post test inspections and drop analysis were 1.9 inches. Further discussion was provided in the response to RAJ 2-17.

To evaluate balsa wood properties for the end drop case, a core sample measurement of the end drop CTU was made to confirm observations presented in the test report. The core sample showed that the balsa block crushed 2 inches. Using the revised material properties for balsa, the end drop analysis agreed with the physical test results. A damage comparison will be added to Appendix 2.12.5 of the SAR.

NRC RAI for RAJ-II Package – Docket No. 71-9309, TAC No. L24456:

2-11 Provide damage comparisons (displacements, stresses, etc.) for FEA models and fuel rods. Peak G loads alone do not provide a complete engineering record with respect to overall package damage or the potential for damage. Staff does not have reasonable assurance that peak G loads alone are sufficient for making a safety determination for this package.

Response:

Evidence that the fuel rods remain intact during HAC is best demonstrated by the information provided in Attachment 3 of the RA-3D test report (III.3/20554). The RA-3D test report provides measurements for actual production fuel bundles. As discussed in RAI 2-10, the LS-DYNA model is benchmarked based on a combination of peak G loads and foam crush distances.

NRC RAI for RAJ-II Package – Docket No. 71-9309, TAC No. L24456:

2-12 Provide sensitivity study demonstrating that rigid fuel payload is conservative. Staff does not have reasonable assurance that the assumption of rigid payload is conservative. Previous analyses performed by NRC staff have indicated that payload stiffness is a significant contributor to package response.

Response:

An LS-DYNA top drop analysis was performed using elastic properties for the fuel bundle payload and compared with data from the original Japanese RAJ-II drop testing program. For both test and analysis, data was collected at accelerometer locations at the center of the fuel bundle. The same solid brick model used for the rigid case was used for the elastic fuel bundle case with a representative modulus of elasticity to simulate the stiffness properties.

Acceleration time histories were recorded at the center of the bundle close to the location of the physical accelerometer in the drop test. Figure 2-12.1 was an overlay of drop test and LS-DYNA analysis results.

As Figure 2-12.1 showed, the Japanese top drop test results (black line) filtered at 500 Hz was compared with LS-DYNA filtered acceleration time-history results ranging from 25 Hz to 500 Hz. The rigid fuel bundle result was also provided for comparison (red line).

Referring to the Japanese top drop, the plot showed additional sinusoidal waves on top of the primary impact responses. This resulted from the actual fuel bundle geometry as the individual rods responded to the impact. The Japanese top drop is also represented by a 6 order polynomial curve fit (gray dashed line). The shape and duration of the curve fit matched the LS-DYNA results.

From results of shaker table testing (fully loaded RAJ-II), road testing vibration studies, flow induced vibration testing of fuel bundles, and seismic testing of fuel bundles, it was determined that the natural frequency of the fully loaded RAJ-II was less than 25 Hz and the fuel bundle was approximately 10 Hz. Using a Butterworth filter and evaluating the results at 25 Hz resulted in a maximum acceleration of 66g. Therefore, performing the evaluation with a rigid fuel payload was conservative for the following reason:

- *All of the energy was absorbed by the crushable materials of the package with no loss to the contents.*
- *The LS-DYNA results were checked by integrating the acceleration time history to verify the velocity thus the kinetic energy.*

- *Using rigid properties avoided the need to aggressively filter the results which in many cases could skew the analysis results, if too few data points were requested for the LS-DYNA NODOUT file.*

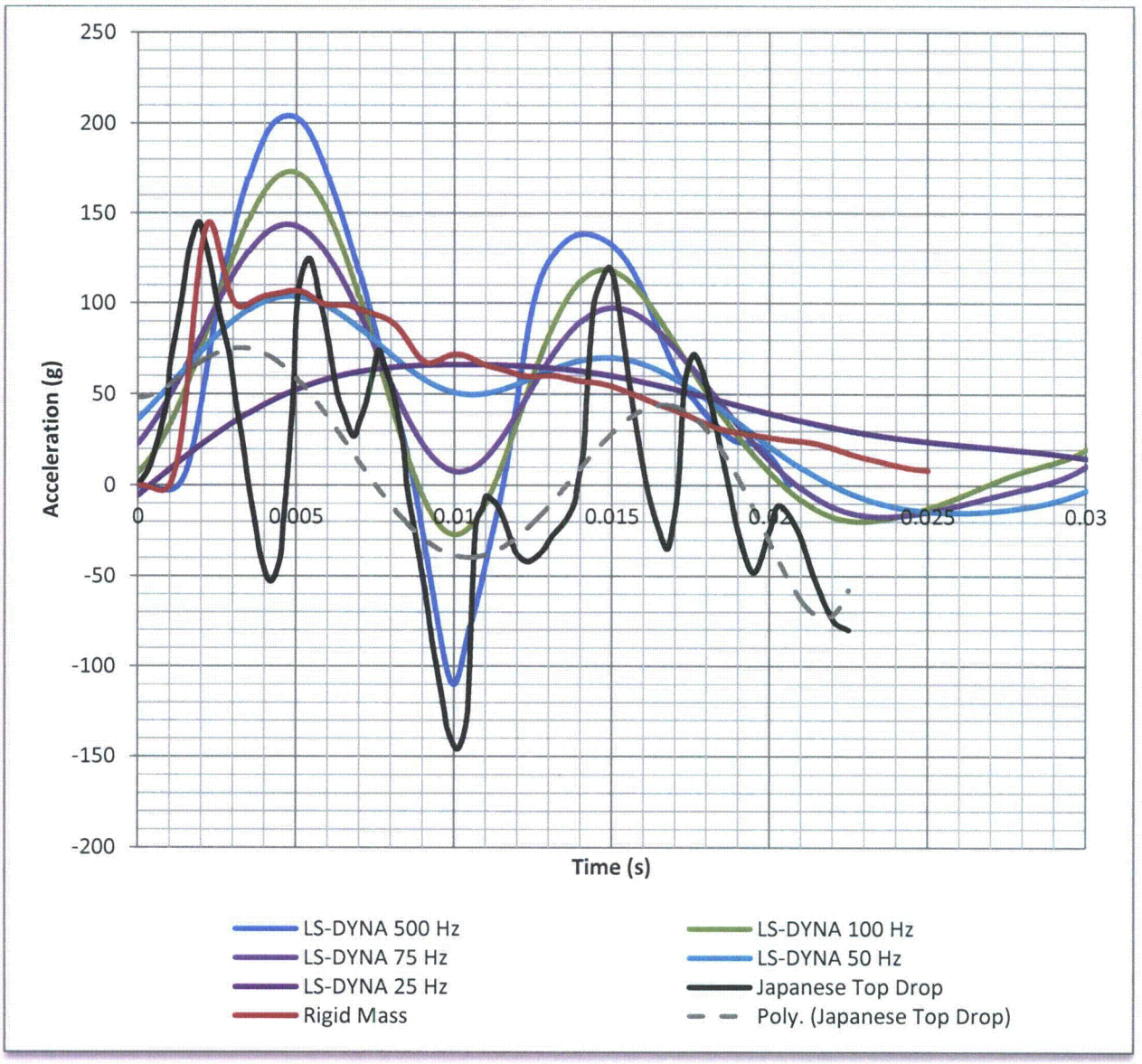

Figure 2-12.1. Comparison of Japanese Top Drop Results and LS-DYNA Analyses

NRC RAI for RAJ-II Package – Docket No. 71-9309, TAC No. L24456:

2-13 Provide a component study that demonstrates correct performance of paper honeycomb material. A simple crush evaluation for a representative honeycomb block when compared with test data provides reasonable assurance that the honeycomb block is providing the correct structural response with appropriate material properties.

Response:

To determine the correct performance of the paper honeycomb material, a simple model was developed. The model was run to show the input stress-strain curves resulted in accurate stress results.

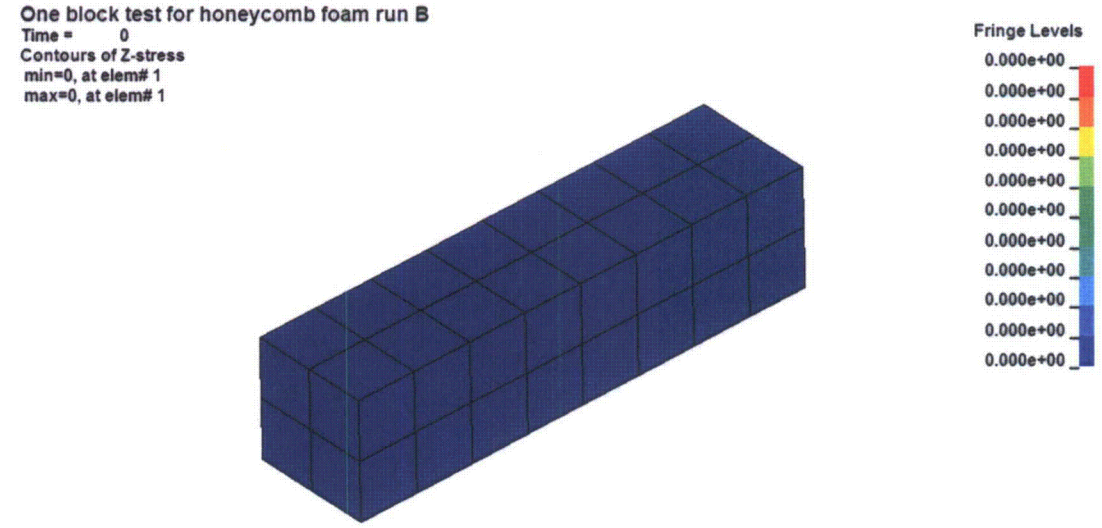

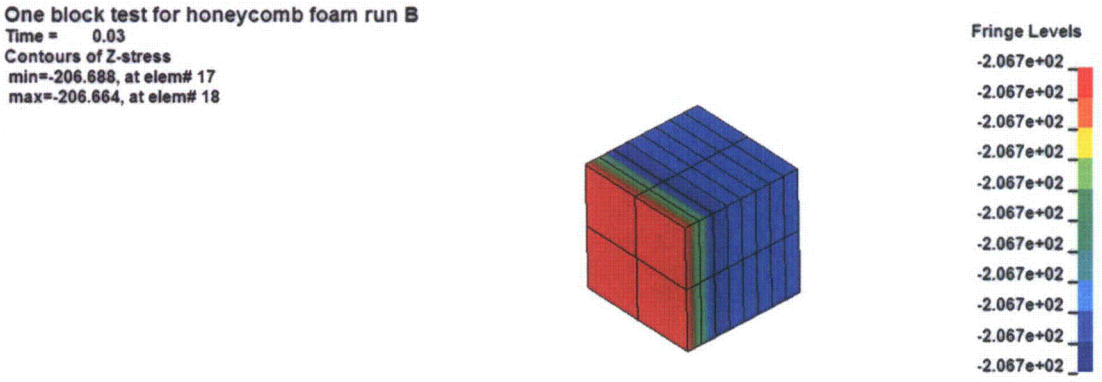

The material model was further refined using the sub-model shown below by benchmarking the honeycomb crush with the drop test results, solving interface and negative volume problems, and verifying total kinetic energy. Further discussion was provided in the response to RAI 2-17. Once this study was complete, the outer container was added to the final model.

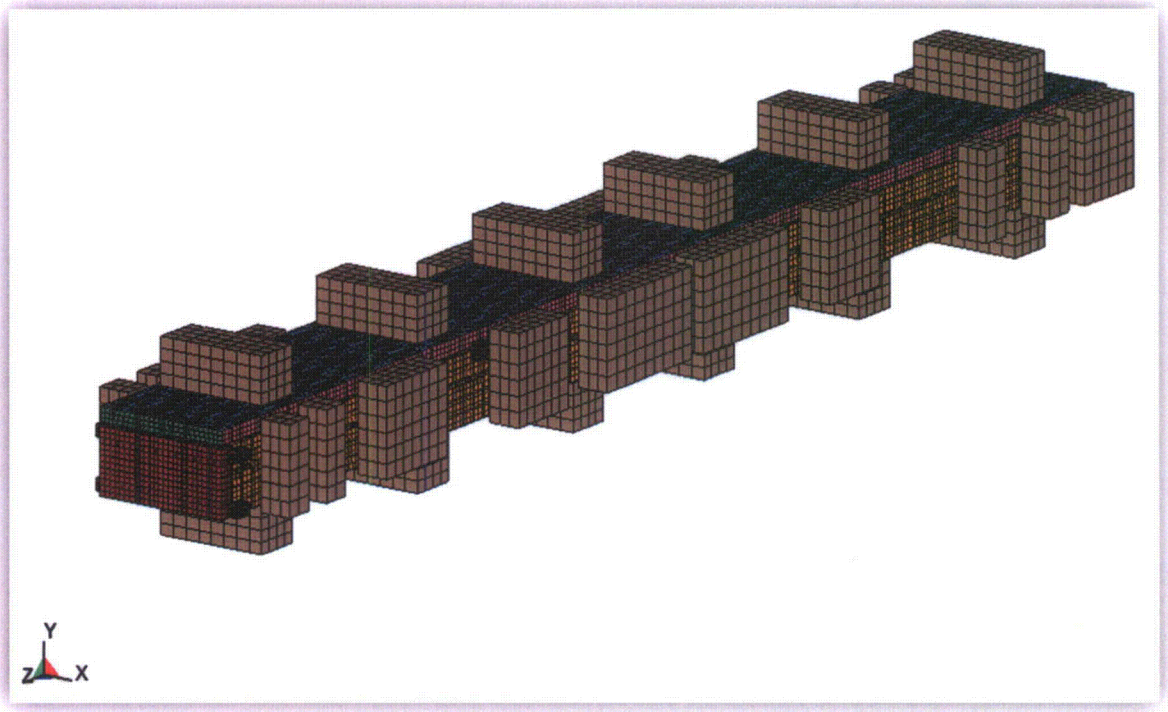

NRC RAI for RAJ-II Package – Docket No. 71-9309, TAC No. L24456:

2-14 Provide dynamic FEA analysis of end drop and CG over corner for RAJ-II. Staff requests this analysis to provide reasonable assurance that the assumptions used in the fuel assembly evaluation are reasonably conservative.

Response:

The response for RAI 2-14 is incorporated into the response for RAI 2-20.

NRC RAI for RAJ-II Package – Docket No. 71-9309, TAC No. L24456:

2-15 Provide comprehensive engineering comparison of the RAJ-II and the RA-3D package to demonstrate similarity. The applicant states that these packages are similar but no objective information is provided to demonstrate that this statement is accurate.

Response:

History of RAJ-II and RA-3D Shipping Containers

The RA series of containers were developed from a common design. The first generation design, known in the United States as the RA-3, consisted of a metal inner container and wooden outer container with honeycomb blocks and Ethafoam to line the inner container providing protection against impact and vibration. Each country adopted the design with minor changes. The Japanese container was named the RAJ, and the German equivalent was named the RA-3D. The RAJ was essentially the same design as the RA-3 with a carbon steel inner container, no thermal insulation, and a wooden outer container. The RA-3D design was an exact copy of the RA-3 with the exceptions of a stainless steel inner container, the addition of lifting trunnions and latches used in place of bolts to secure the inner container lid.

In the early 1990's the Japanese developed the RAJ-II as the second-generation BWR container based on the lessons learned from the previous design. Because of concerns about decontamination and maintenance, the wooden outer container was replaced with stainless steel. An additional improvement to the outer container included the addition of a vibration isolation frame that reduced the amount of high cycle vibrations to the fuel bundles during normal transportation.

Because of limitations at the customer facility, the RAJ-II inner container design was changed little from the original RA-3. Like the RA-3D, the RAJ-II inner container was constructed of stainless steel. Unlike the RA-3D, the RAJ-II inner container included Alumina-Silicate insulation to protect the fuel bundles during the regulatory fire event. Figures 2-15.1 and 2-15.2 show the design features of the RAJ-II and RA-3D, respectively.

Detailed Comparison

The following compares the design features of the RAJ-II and RA-3D:

1. Dimensionally, the RA-3D is almost identical to the RAJ-II inner container in length, width, and height.

2. Testing shows that the bundles act as lumped masses supporting first principle basics that the impact is mass driven. Since both RAJ-II and RA-3D containers ship the same fuel designs, the same lump mass principle applies to both designs.
3. Both containers are designed for the same fuel bundle designs.
4. The RA-3D and RAJ-II inner containers are constructed of 300 series stainless steel.
5. The overall construction of the RA-3D and the RAJ-II is very similar. Both containers are formed and welded of similar sheet metal construction containing an inner and outer skin of similar thicknesses.
6. Both containers use Ethafoam to protect the fuel bundles.
7. Both containers are designed to carry 2 fuel bundles.
8. Both outer containers use honeycomb blocks for impact resistance.
9. The bending resistance about the inner container weak axis is nearly the same. The area moments of inertia for the RAJ-II and RA-3D are 8,909 cm4 and 9,313 cm4, respectively.
10. The RAJ-II has a vibration isolation frame that prevents the inner container from shifting during handling and transportation. The RA-3D inner container is free to shift inside of the outer container.
11. The RAJ-II uses Alumina-Silicate as thermal insulation.
12. The RAJ-II has a stainless steel outer container to protect the fuel during accident conditions. The RA-3D outer container is constructed of wood.
13. The RAJ-II all stainless steel construction allows easy decontamination with minimal maintenance.

Conclusion

Because of the many similarities between the RA-3D and RAJ-II designs and because both containers ship the same BWR fuel types, the RA-3D test results are acceptable for use in determining the performance of the RAJ-II during impact events.

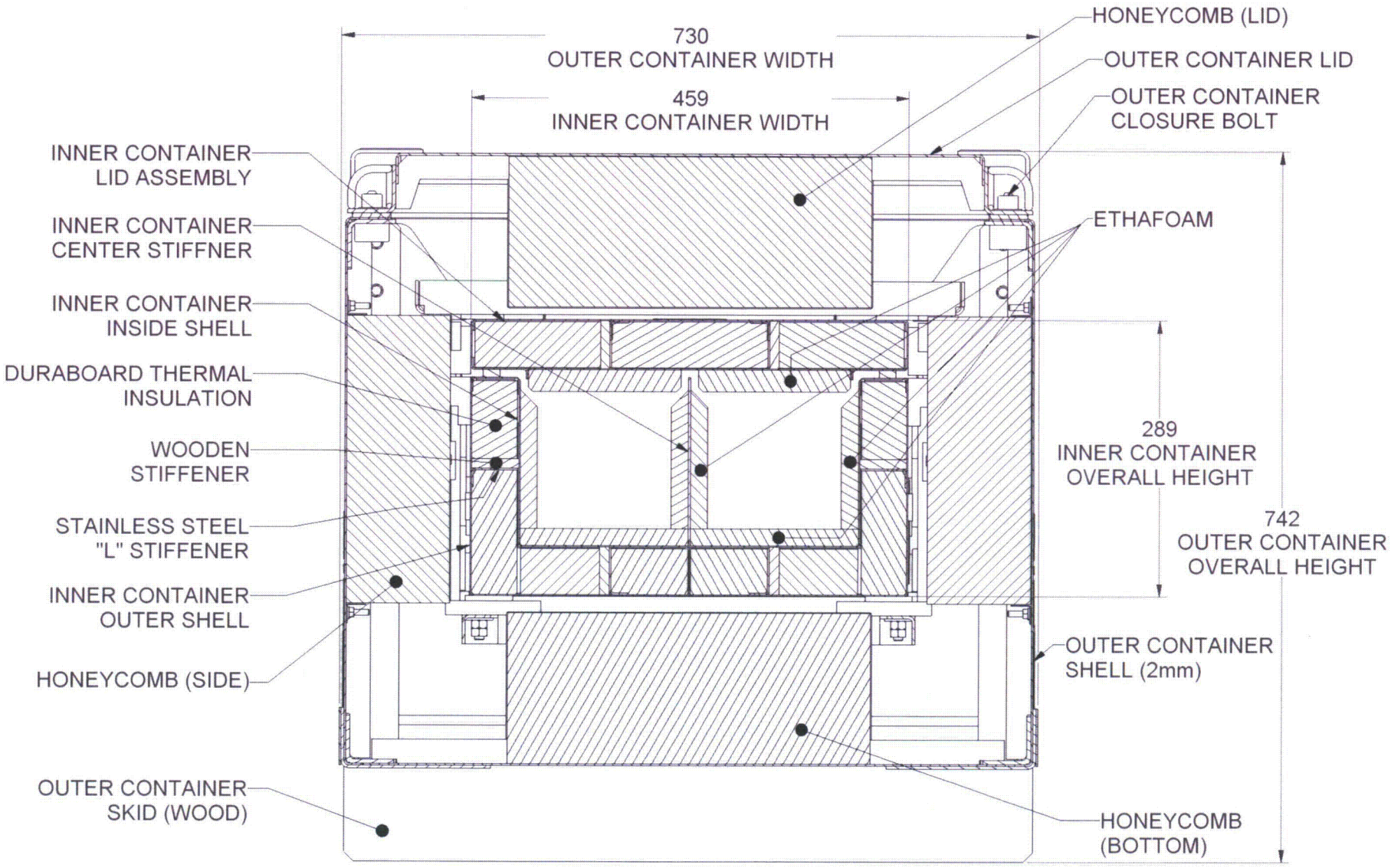

Figure 2-15.1 Cross-Section RAJ-II Package

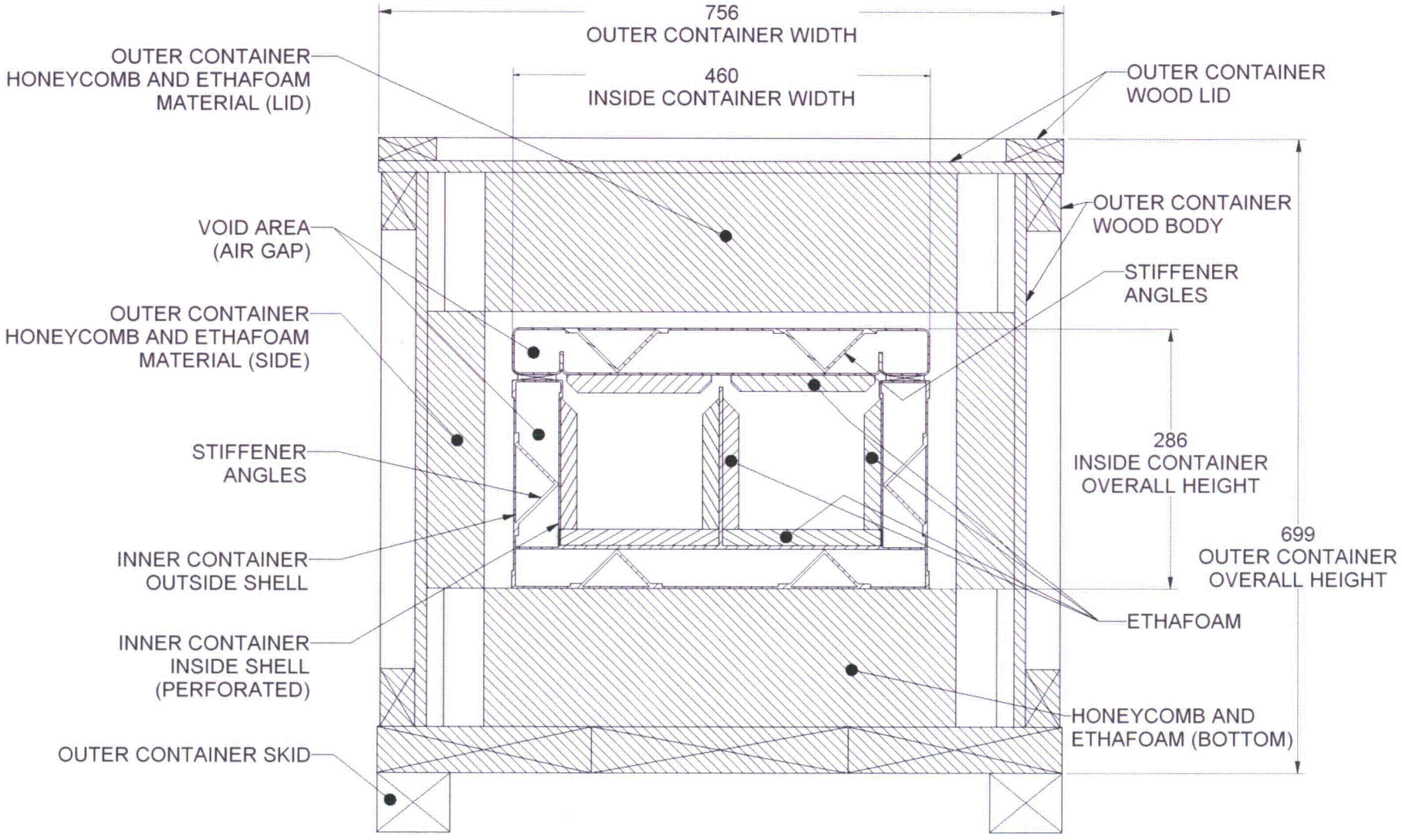

Figure 2-15.2 Cross-Section RA-3D Package

NRC RAI for RAJ-II Package – Docket No. 71-9309, TAC No. L24456:

2-16 Provide dynamic FEA analysis(es) of the RA-3D. Since the RA-3D is being represented as a reasonable analogue of the RAJ-II, staff requests that a representative sample of analytical models be provided to demonstrate the similarity.

Response:

Finite element models of the RA-3D were not developed because of the availability of complete test data. As concluded in the response to RAI 2-15, the RA-3D provided a good analogue to the RAJ-II. In response to this RAI, GNF obtained permission from the German authority BAM to provide the NRC with the complete test report (III.3/20554). GNF will provide a hard copy of the test report with annotation to assist the NRC with the document layout. The RA-3D testing provided a unique insight into the response and performance of actual natural uranium fuel bundles during regulatory test conditions.

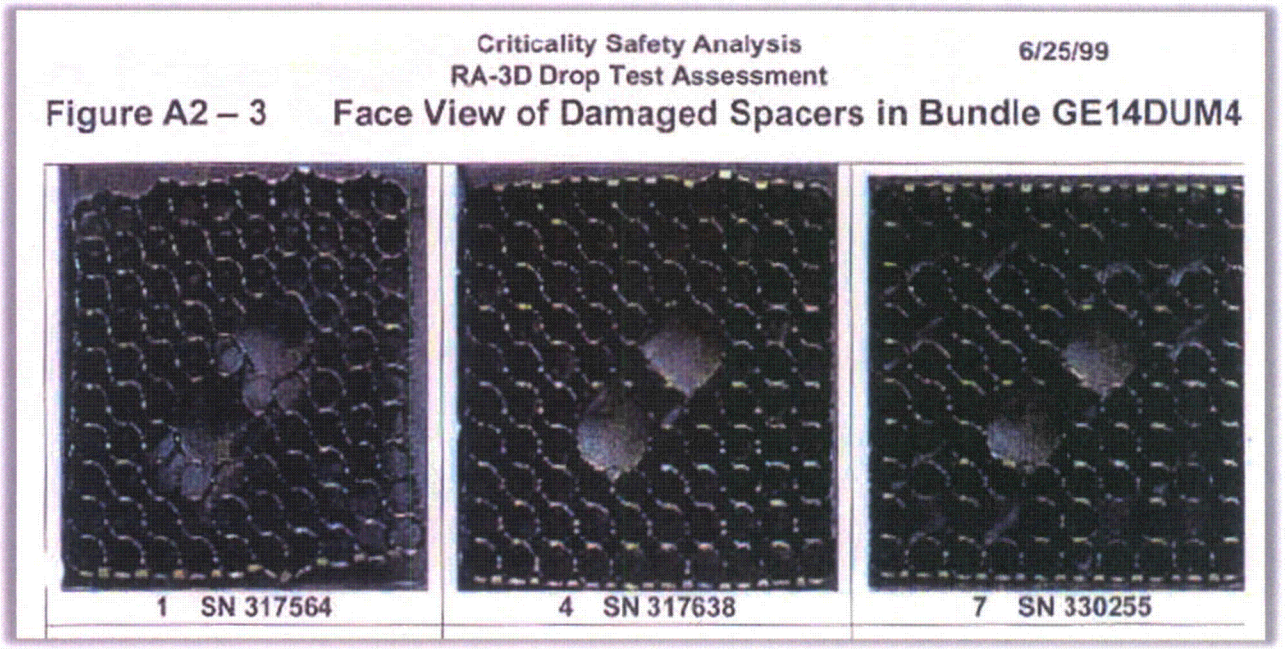

NRC RAI for RAJ-II Package – Docket No. 71-9309, TAC No. L24456:

2-17 Justify the tuning of the modulus of elasticity of the paper honeycomb to achieve a peak G load of 145Gs. Tuning material properties to achieve desired results is not considered a best practice when attempting to benchmark an analytical model against a test. Absent an evaluation of other test markers for damage such as deformation or strain, which would indicate that published values for elastic modulus are erroneous, this practice is not considered a reasonable approach for benchmarking.

Response:

The term tuning the modulus was inappropriately applied in the SAR discussion. In reality the modulus for the honeycomb and foam were derived from a series of laboratory test samples giving a range of modulus values. The first attempt at deriving a modulus assumed a simple average value of the test samples based on static load tests. The resulting analysis was adequate; however peak acceleration values were approximately 5% below the peak acceleration of 145Gs recorded during the top drop test. Therefore, a stiffer modulus value was chosen within the tested values that matched the test results to account for the strain-rate effects and provided a good baseline point to compare to for all future analyses.

Benchmarking of the results was accomplished by comparing the measured crush values of the honeycomb post drop test with a series of honeycomb nodal displacements along the length of the lid. Because of the interaction between the lid and honeycomb, the height of the honeycomb post impact measurements ranged between 1.7 and 2.13 inches. The average post impact height value for both the post test inspections and drop analysis was 1.9 inches. Additionally, when rigid properties were used to model the payload, the initial velocity was confirmed from the output and total kinetic energy calculated. Therefore, the direct relation between honeycomb displacement and total kinetic energy absorbed was used to verify the material model.

NRC RAI for RAJ-II Package – Docket No. 71-9309, TAC No. L24456:

2-18 Clarify the following discrepancy: On p 2-90 reference is made to the RAJ-III top drop test, which refers back to Section 2.12.2.3. Section 2.12 specifically references certification tests on the RAJ-II.

Response:

The reference to the RAJ-III top drop test is a typographical error. The reference to 2.12.2.3 is corrected. Of the two RAJ-II drop testing programs, only the Japanese program collected accelerometer data. The reference will be corrected and reference to the RA-3D drop testing program will also be made.

NRC RAI for RAJ-II Package – Docket No. 71-9309, TAC No. L24456:

2-19 Provide accelerometer locations on both tested CTUs and acceleration time history sampling points on FEA models. This information is necessary for evaluating the robustness of the analytical model in capturing dynamic behavior.

Response:

The following table provides a summary of the available drop test data and accelerometer location. Comparison of the sensor location between the CTU and FEA model is provided with each CTU and FEA overlay plot provided in response to RAI 2-20.

Table 2-19.1. Package Drop Test Orientation and Accelerometer Location

Package	Test Location	Drop Orientation	Acceleration (G)	Sensor Location	Figure #
RAJ-II	Japan	Horizontal top drop	145	Center of bundle	2-20.1
RAJ-II	Japan	Horizontal top drop	194	Inner container outer shell	2-20.2
RA-3D	Spain	Horizontal side drop	487	Upper tie plate	2-20.3
RAJ-II	Japan	Vertical end drop	303	Inner container outer shell	2-20.4
RAJ-II	Japan	Vertical CG over corner	203	Lower tie plate	2-20.5
RA-3D	Spain	Vertical CG over corner	195	Inner container outer shell	2-20.5

NRC RAI for RAJ-II Package – Docket No. 71-9309, TAC No. L24456:

2-20 Provide overlay plots of the acceleration time histories for CTUs and FEA models. Acceleration time history shape as well as peak values are important to verify whether an analytical model is sufficiently robust to capture dynamic behavior.

Response:

The following curve shows the results of Japanese top drop test and LS-DYNA analysis results. The sensor location for both the analysis and test was on the fuel bundle. As the test curve shows, the sensor recorded the elastic response of the bundle during the impact. This data was chosen as the initial benchmark to verify the LS-DYNA honeycomb model with the drop test results. As discussed in the response to RAI 2-17, the measured crush of the honeycomb was 1.9 inches.

Figure 2-10.1. Comparison of RAJ-II Top Drop and LS-DYNA results (Center of Bundle).

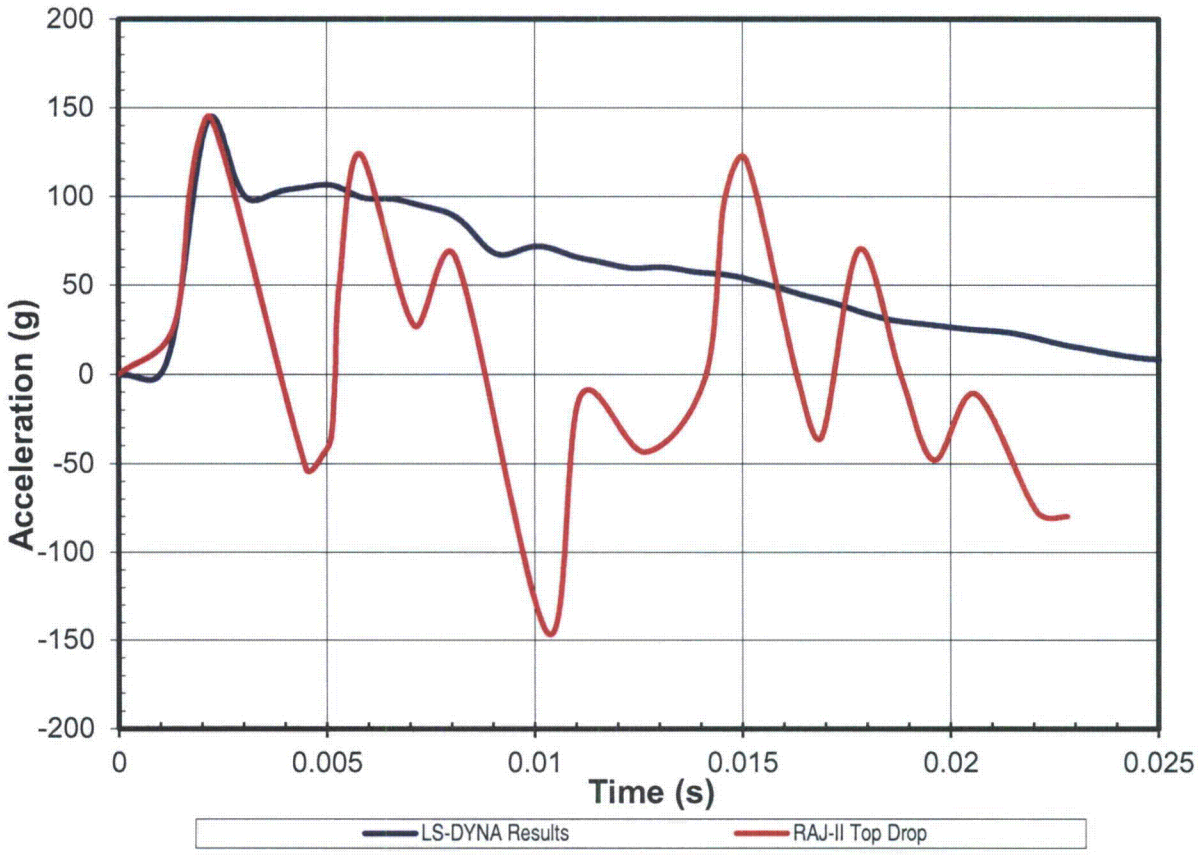

The following figure is a comparison of the Japanese RAJ-II top drop with the accelerometer located on the side of the inner container. Because the exact location of the sensor is not documented, an average of 4 nodes along the length of the inner container is used to represent the LS-DYNA responses. The LS-DYNA results show good agreement with the drop test results.

Figure 2-10.2. Comparison of RAJ-II Top Drop and LS-DYNA results (Inner Container Shell).

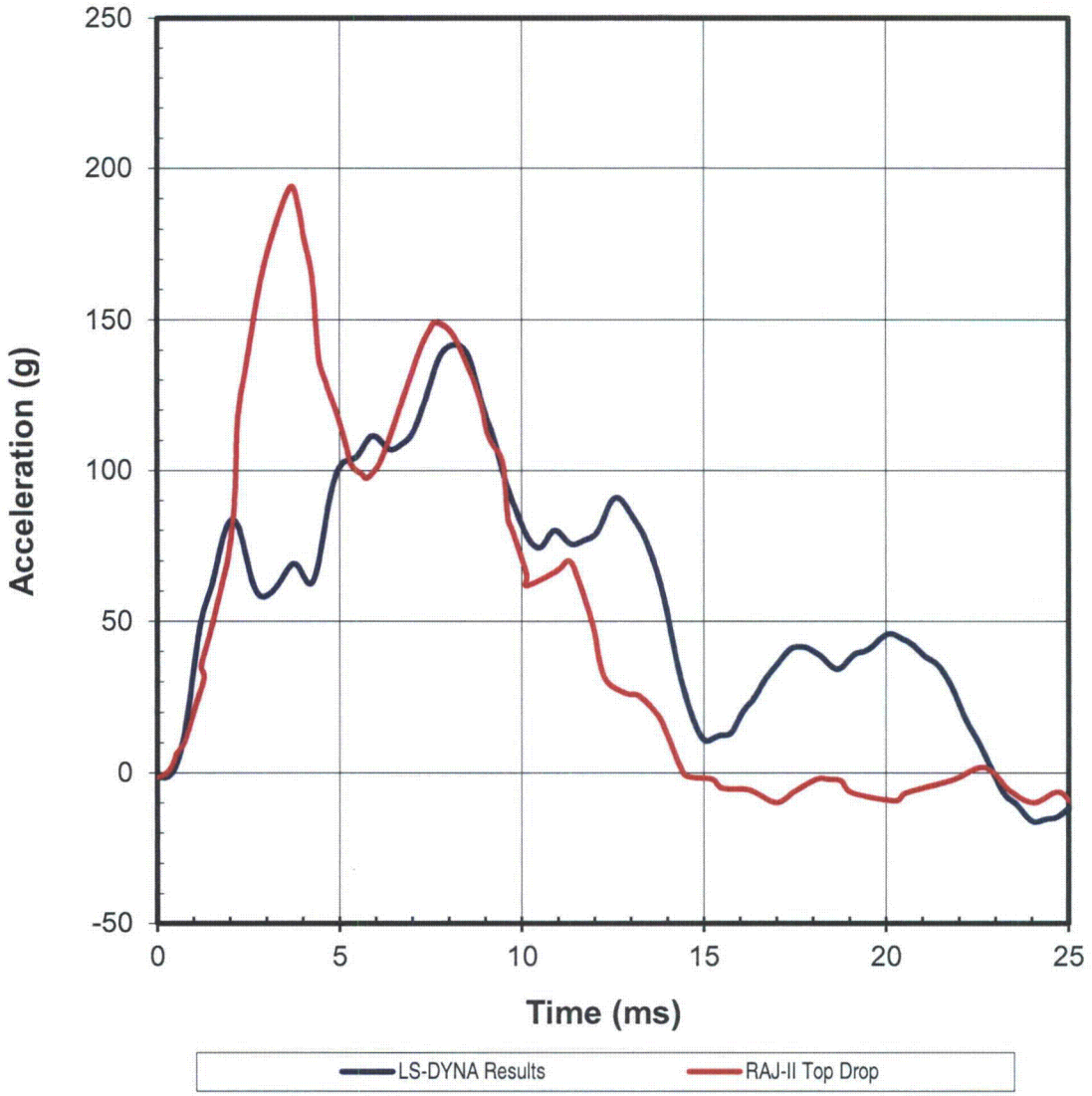

Following the completion of the top drop analysis, where the material properties were benchmarked, the honeycomb properties were copied to the side drop model and the side drop analysis was completed. However, accelerometer data was not available for the side drop case during either of the two RAJ-II testing programs. The best comparison for the RAJ-II side drop case was the data available from the Spanish test program for the RA-3D (see also response for RAI 2-15). As the following figure shows, the LS-DYNA analysis properly captured the response of the initial impact and subsequent secondary responses of the fuel bundles, as the crushable materials in the inner container deformed and the inner container flexes.

Figure 2-10.3. Comparison of RA-3D Side Drop and LS-DYNA results.

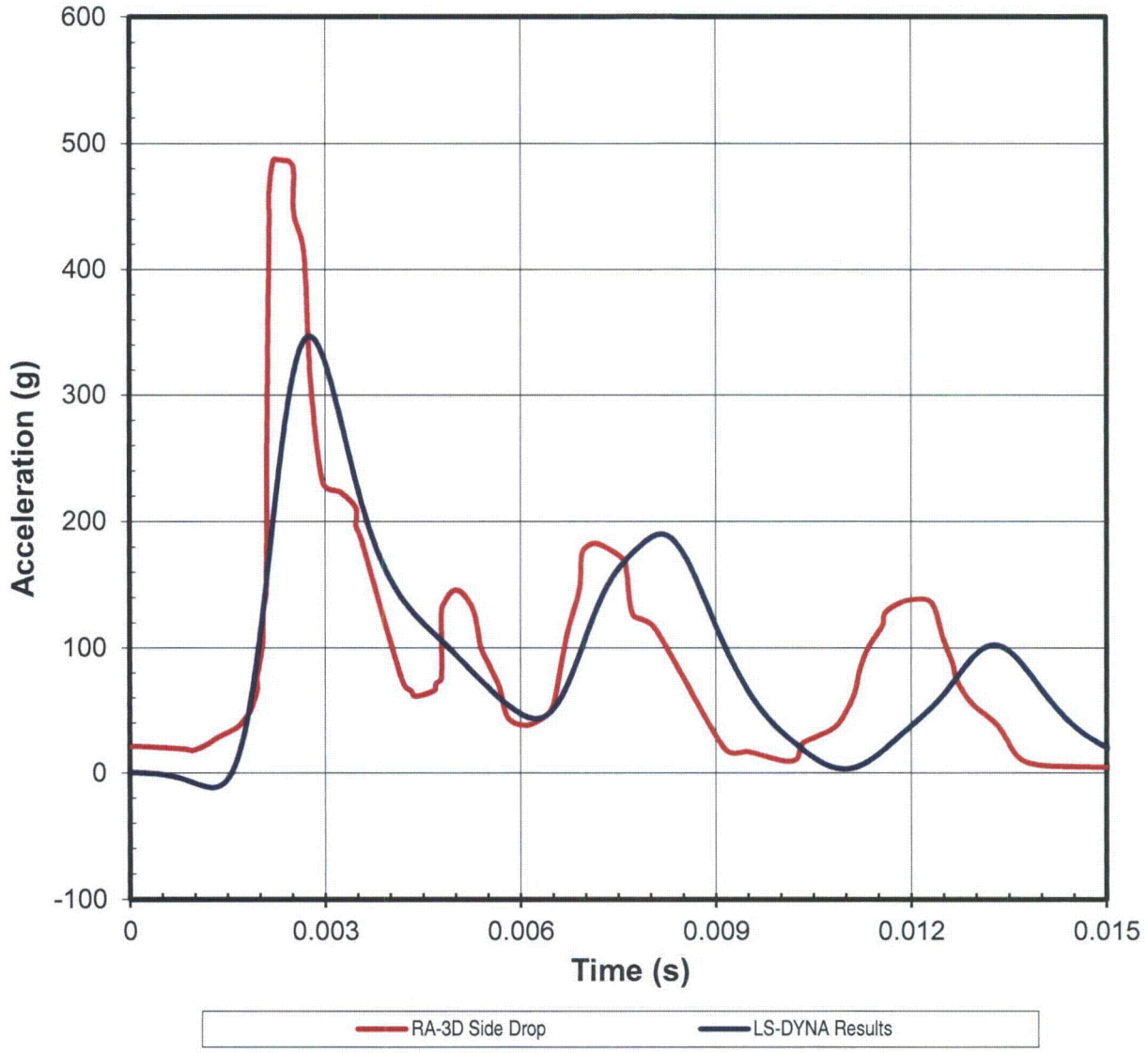

The following figure represents the end drop of the package and the crushing of the balsa blocks located at the end of the container. Benchmarking of the balsa properties was accomplished by taking measurements from the balsa post impact and comparing to the LS-DYNA results. Evaluation of the CTU shows that a maximum crush of 2 inches occurs under the point of impact which agrees with the LS-DYNA results.

Figure 2-10.4. Comparison of RAJ-II End Drop and LS-DYNA results.

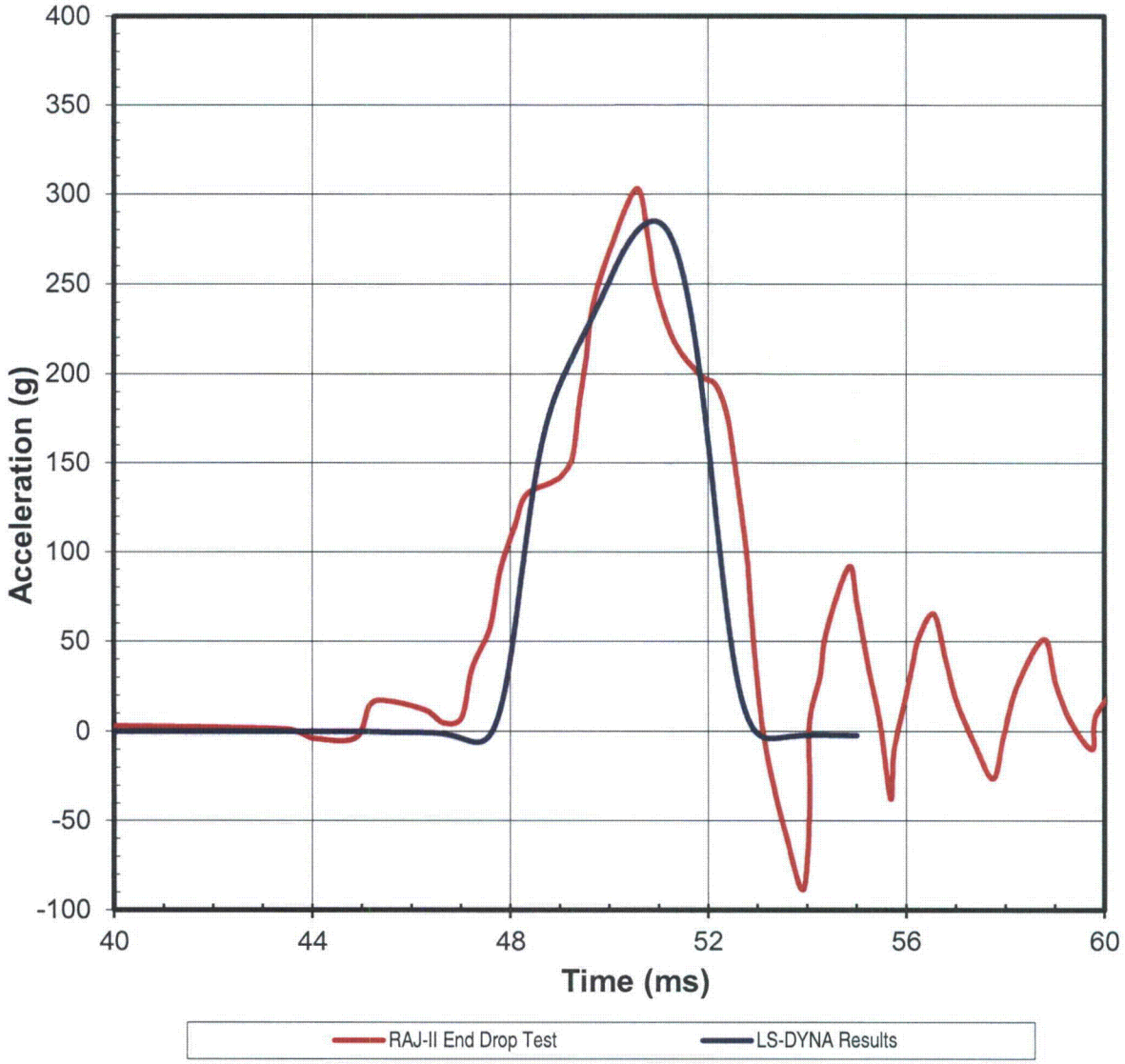

Using the balsa properties used for the end drop case, the corner drop evaluation was performed. As the results shows, the magnitude, and pulse duration compared favorably with the Japanese RAJ-II corner drop and RA-3D corner drop cases. It was observed that the corner drop acceleration is less than the end drop because of corner deformation at the point of impact and the smaller initial contact area.

Figure 2-10.5. Comparison of RAJ-II Corner Drop and LS-DYNA results

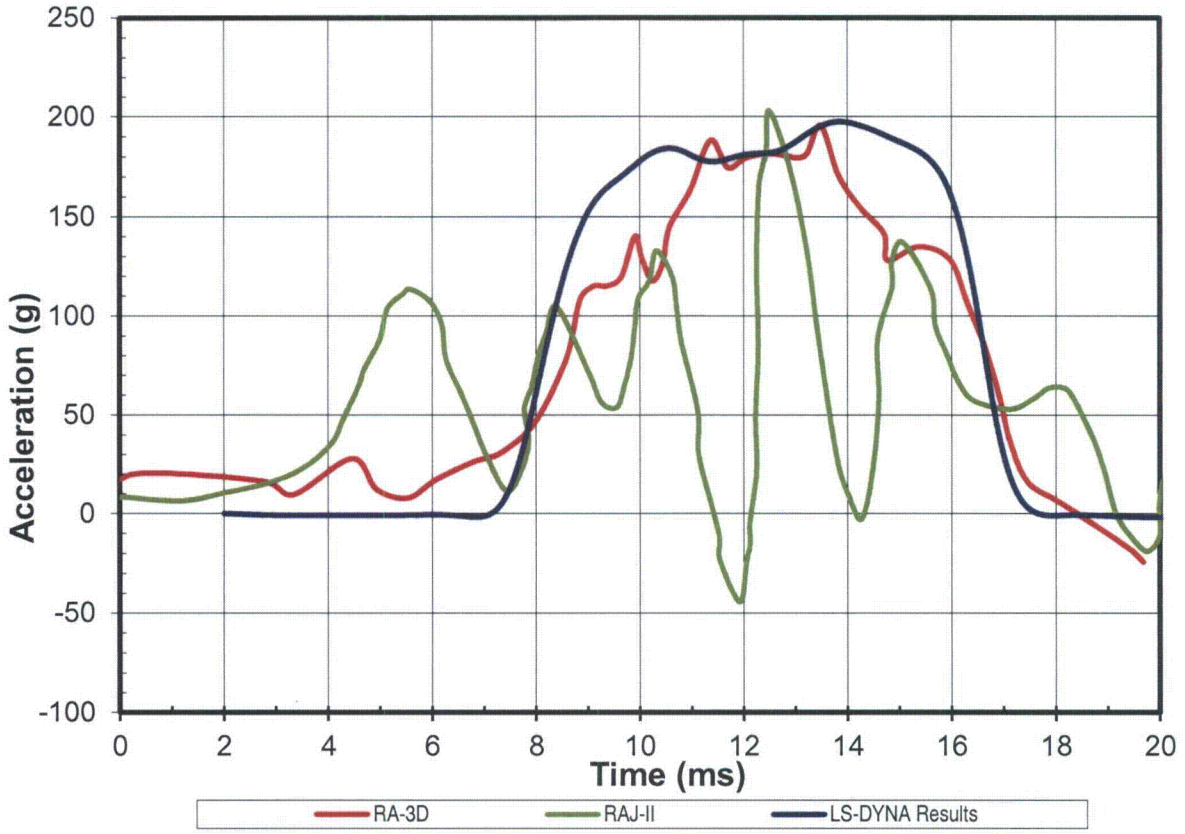

NRC RAI for RAJ-II Package – Docket No. 71-9309, TAC No. L24456:

2-21 Demonstrate that the delay of leak testing due to transport did not result in a "false negative" leak test. Section 2.12.1.3, "Test Performance," indicates that the CTU packages were tested at Oak Ridge and then transported to Lynchburg, Virginia, where they were disassembled, examined, and leak tested. Staff is concerned that the delay in leak testing could have resulted in no detection because no gas would remain in or around the fuel rods after the period of time required for transport.

Response:

Leak testing of the fuel rods occurred approximately 5 days after the drop test in Oak Ridge. Upon arrival at the Lynchburg facility, Areva personnel and NRC inspector performed detailed examination of the test bundle. Following the inspection, the bundle was leak tested using standard procedure. Because of the extreme sensitivity of the leak test equipment (of 1×10^{-8} cc/sec atm range), individual helium atoms could be detected. If cracks or pin holes in the cladding had occurred, sufficient helium would remain behind to provide accurate test results.

NRC RAI for RAJ-II Package – Docket No. 71-9309, TAC No. L24456:

Criticality Safety:

RAI 6-1:

Revise the application to clearly state the dimensions of each fuel assembly and rod type to be transported in the Model No. RAJ-II package, as well as the tolerances for each of these dimensions that have been evaluated in the criticality safety analysis. Include in the list of dimensions and tolerances: pellet diameter, clad thickness, rod outer diameter, maximum active length (for full and partial rods), and rod pitch.

Although the applicant provided a list of rod nominal dimensions in Appendix 6.9.5, and a sample of assembly parameters in Section 1.3 of the SAR, the specific fuel contents and their associated dimensions remain unclear. Additionally, although the applicant provided an evaluation of material uncertainties in the criticality analysis, it is not clear how the uncertainties evaluated translate into dimensional tolerances that can be referenced in the Certificate of Compliance. Note that the aforementioned dimensions and their associated tolerances will be included as limits in the package Certificate of Compliance in order to prevent shipment of contents that have not been evaluated in the, criticality analysis.

Response:

For clarification of the fuel design specifications carried through to the criticality safety analysis, a summary of the data represented in Ch. 1 will be added to new section in Chapter 1, as shown in below. The tolerances will be specified in Ch. 6. It is proposed for the CoC, that Table 1-X will be included containing fuel specs and tolerances (additional table row shown below Table 1-X).

1.3.3.3 Summary of Fuel Designs

Table 1-X provides a summary of GNF and Westinghouse fuel bundle types applicable for package contents. Note water rod and partial length fuel rods positions are in relation to Figure 6-X.

Table 1-X – BWR Fuel Bundle Parameters and Tolerance

Fuel Design	Fuel Pellet OD (cm)	Fuel Rod Height (cm)	Cladding ID (cm)	Cladding OD (cm)	Pitch (cm)	Water Rod Positions	Partial Length Fuel Rod Short Height, Positions	Partial Length Fuel Rod Long Height, Positions
GE11 9x9	0.956	370.84	0.975	1.118	1.438	E-4 F-4 D-5 E-5 F-5 D-6 E-6	--	243.84 cm B-2 E-2 H-2 B-5 H-5 B-8 E-8 H-8
GE12B 10x10	0.876	405.5	0.894	1.026	1.295	F-4 G-4 F-5 G-5 D-6 E-6 D-7 E-7	--	259.61 cm B-2 D-2 G-2 I-2 B-4 I-4 E-5 F-6 B-7 I-7 B-9 D-9 G-9 I-9
GE13 9x9	0.956	370.84	0.975	1.118	1.438	E-4 F-4 D-5 E-5 F-5 D-6 E-6	--	274.32 cm B-2 E-2 H-2 B-5 H-5 B-8 E-8 H-8
GE14C 10x10	0.876	381	0.894	1.026	1.295	F-4 G-4 F-5 G-5 D-6 E-6 D-7 E-7	--	243.84 cm B-2 D-2 G-2 I-2 B-4 I-4 E-5 F-6 B-7 I-7 B-9 D-9 G-9 I-9
GE14G 10x10	0.876	370.84	0.894	1.026	1.295	F-4 G-4 F-5 G-5 D-6 E-6 D-7 E-7	--	B-2 D-2 G-2 I-2 B-4 I-4 E-5 F-6 B-7 I-7 B-9 D-9 G-9 I-9
GNF2 10x10	0.888	381	0.906	1.026	1.295	F-4 G-4 F-5 G-5 D-6 E-6 D-7 E-7	137.2 cm E-4 D-5 E-5 F-6 G-6 F-7	259.1 cm E-1 F-1 A-5 J-5 A-6 J-6 E-10 F-10
SVEA-96 10x10	0.848	390	0.863	0.984	1.28	E-5 F-5 E-6 F-6	130 cm E-4 F-4 D-5 G-5 D-6 G-6 E-7 F-7	240 cm A-1 J-1 A-10 J-10

Added as last row to Table 1-X above for CoC contents specification

Fuel Design	Fuel Pellet OD (cm)	Fuel Rod Height (cm)	Cladding ID (cm)	Cladding OD (cm)	Pitch (cm)	Water Rod Positions	Partial Length Fuel Rod Short Height, Positions	Partial Length Fuel Rod Long Height, Positions
Tolerance	0.2%[a]	Listed as max	1% [b]		1% of nominal listed [c]	--	--	--

NOTE: Reference Drawing [a] AA284999; [b] AA294145; [c] AA273878

RAI 6-2:

Revise Section 6.1.2.1 of the SAR to clarify the statement regarding fuel lattices that do not have fissile material.

Criteria number five for restraints on the placement of burnable absorber (BA) rods states that "No BA rods are required in fuel lattices that do not have fissile material (natural uranium defined as uranium containing a mass percentage of uranium-235 that does not exceed 0.72%) or is fissile excepted (uranium enriched in uranium-235 to a maximum of 1% by weight)." The SAR should be revised to clarify that fuel assemblies which are non-fissile or exempted from the fissile material requirements of 10 CFR 71.15 are intended as allowable contents in the package.

Response:

Text changed in Section 6.1.2.1 for clarification, as follows:

6.1.2.1 Fuel Bundle or Fuel Assembly

5. No BA rods are required in fuel lattice zones (i.e., axial zones) that do not have fissile material (natural uranium defined as uranium containing a mass percentage of uranium-235 that does not exceed 0.72%) or is fissile excepted (uranium enriched in uranium-235 to a maximum of 1 percent by weight).

RAI 6-3:

Revise Section 6.2 of the SAR to clarify the enrichment and gadolinium content of the BA rods required for fuel assemblies with BA rods.

Item three under the description of the fissile material contents states that "A minimum number of eight gadolinium oxide fuel rods with a minimum 2.0 weight percent is assumed for the BA rods in every lattice zone of the fuel bundle." It is unclear if the 2.0 weight percent refers to the gadolinium oxide content or the 235U enrichment. Revise this SAR section to clarify.

Response:

Text changed in Section 6.2 for clarification, as follows:

6.2 FISSILE MATERIAL CONTENTS

3. A minimum number of eight burnable absorber fuel rods with a minimum 2.0 weight percent gadolinium oxide is assumed for the BA rods in every lattice zone of the fuel bundle.

RAI 6-4:

Revise Figure 6-3 of the SAR to include a similar schematic for one of the 9x9 fuel assemblies (either the GE11 or GE13).

This figure provides a schematic layout for several 10x10 fuel assemblies, but does not provide a similar representation of the 9x9 fuel assembly contents. The SAR should be revised to show a representation of the 9x9 fuel assembly.

Response:

Figure 6-3 updated to include 9x9 fuel layout, as follows:

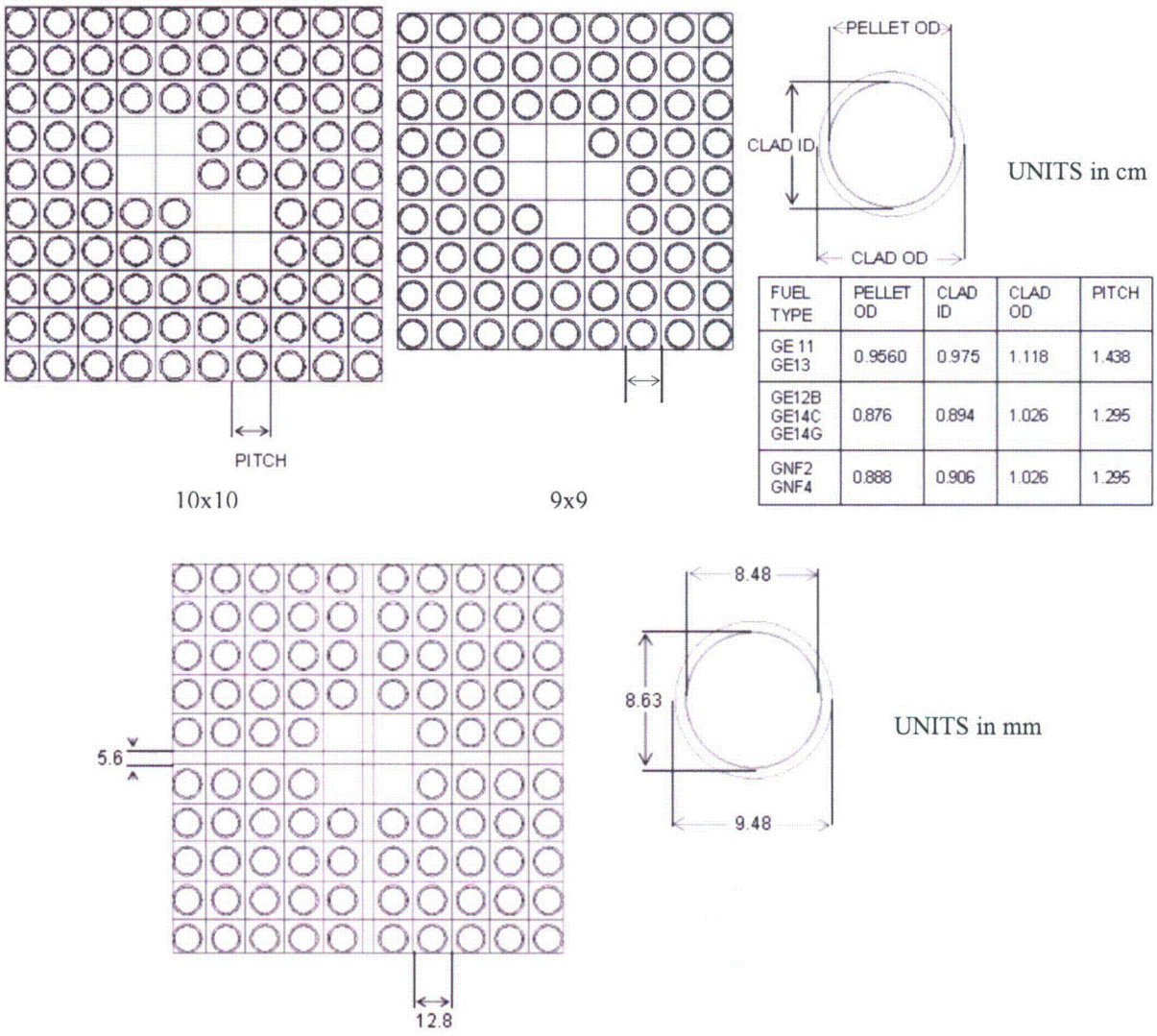

FUEL TYPE	PELLET OD	CLAD ID	CLAD OD	PITCH
GE11 GE13	0.9560	0.975	1.118	1.438
GE12B GE14C GE14G	0.876	0.894	1.026	1.295
GNF2 GNF4	0.888	0.906	1.026	1.295

Figure 6-3 Fuel bundle model – GNF 10x10 and 9x9 (top) and Westinghouse 10x10 (bottom)

RAI 6-5:

Revise Section 6.3.1.1 of the SAR to clarify the dimensions of the protective case. This section states that the height of the protective case is 84 centimeters, and appears to be a typographical error. Revise this section to include the actual height of the protective case.

This information is needed to ensure that the packaging is adequately described, per 10 CFR 71.33.

Response:

Text changed in Section 6.3.1.1 to correct dimensions, as follows:

6.3.1.1 Protective Case, 2nd paragraph update

...

The protective case is a SS body holding the fuel rods, surrounded by a poly urethane cushioning material. The length of the body has exterior dimensions of 9.7 cm wide by 8.9 cm tall by 417.6 cm long, composed of 0.4 cm thick SS. The top lid is installed on top of the body and run the length of the case, composed of 0.5 cm thick SS, resulting in an overall case height of 93 cm. The end plates are 0.5 cm thick SS, and result in a modeled case length of 418.6 cm. Assembly pieces such as the lumber shock absorbers, exterior cushioning materials, and structural steel components are conservatively neglected.

RAI 6-6:

Revise the criticality analysis to justify the assumption of char density considered in the model configuration.

Section 6.3.2.9 of the SAR states that the theoretical density of char is assumed to be 2.1 g/cc, but does not state why this value is chosen and if it is conservative or not. The SAR should be revised to justify this assumption.

This information is needed to ensure that the package will meet the criticality safety requirements of 10 CFR 71.55(e) for single packages under hypothetical accident conditions, and of 10 CFR 71.59 for package arrays.

Response:

The purpose of evaluating the effect of char is to consider the effect of a moderating material that is more effective than water in the void space of the packaging. Other studies have demonstrated that representing the carbon density the same as amorphous carbon results in higher k-eff (Ref. Criticality Assessments Of Polyurethane Foam, James Lam Physicist, Rolls-Royce plc. PO Box 2000, Derby, DE21 7XX, United Kingdom PATRAM 2010, London). Although, the description of the carbon in Section 6.3.2.9 identifies a theoretical density for carbon, the carbon number densities used in the evaluation are the same that for the material prior to thermal decomposition. The actual carbon number densities are in Table 6-8, Summary of Material Compositions.

Paper Honeycomb $C_6H_{10}O_5$	0.08	C-12 H-1 O-16	1.78300E-03 2.97167E-03 1.48583E-03
Char (Paper Honeycomb)	0.036	C-12	1.78300E-03
Balsa Wood $C_6H_{10}O_5$	0.125	C-12 H-1 O-16	2.78594E-03 4.64323E-03 2.32161E-03
Char (Balsa wood)	0.056	C-12	2.78594E-03

RAI 6-7:

Revise Section 6.6.2.1.2 of the SAR to clarify the rod pitches evaluated for the fuel rods without rod containers.

Table 6-37 of this section shows evaluated rod pitches of rod outer radius, 1.3 inches, and 1.6 inches, with reported keff increasing with pitch. The SAR should clarify that this largest pitch evaluated is the largest that the inner container will allow for the 25 rod limit. Additionally, if this is the largest pitch allowed by the package dimensions, the SAR should demonstrate that larger pitches with fewer rods are not more reactive.

This information is needed to ensure that the package will meet the criticality safety requirements for package arrays in 10 CFR 71.59.

Response:

Note: this response also addresses the item of pitch type justification (RAI 6-12) for fuel rod shipments without a rod container.

Fuel rods may be transported either packaged in a rod container or as a cluster of fuel rods without a rod container. The package array with fuel rod contents is evaluated using the BWR_G3 fuel rod category, determined as the most reactive category in the infinite rod array comparison (See Appendix 6.9.5). Additionally the minimum (PWR_W5) and maximum (PWR_W3) fuel rod categories as based on fuel pellet diameter are evaluated for the fuel rod contents. For fuel rod shipment without a rod container, a maximum of 25 fuel rods in each compartment of the inner container is permissible. The contents are evaluated through the optimum rod pitch for a cluster of 25 fuel rods to the maximum full pitch of the IC, which is equivalent to 1.76 cm half-pitch for square pitch and 1.6 for hexagonal pitch. Additionally for the fuel rod contents without a rod container, fewer than 25 rods in each inner container compartment are evaluated at pitches optimized to the IC size (see Figure 6-Xa for pitch comparison).

Table 6-37a displays the comparison of the fuel rod categories is shown for a maximum of 25 fuel rods in each compartment of the inner container at several pitches including the limiting maximum full pitch of the IC, and then the increasing pitch and reduction of fuel rods. The maximum k_{eff}, irrespective of pitch type, is used to define the most reactive loose fuel rod case per container.

Table 6-37a 144 package array, No Rod Container, Fuel Category Comparison

No. of rods per IC side	Fuel Category	BWR_G3		PWR_W5 minimum		PWR_W3 maximum	
	Half-Pitch (cm)	k_p	σ_p	k_p	σ_p	k_p	σ_p
25	Rod OR (with NPM) [b]	0.43322	0.00029	0.39644	0.0003	0.45934	0.00027
25	1.3 [b]	0.73709	0.00033	0.67505	0.0003	0.77324	0.00034
25	1.6 [a]	0.75877	0.00031	0.68578	0.0004	0.80154	0.00034
25	1.60-hex; 1.76-sq [a]	0.75877	0.00031	0.68578	0.0004	0.80154	0.00034
22	1.60-hex; 1.76-sq [a]	0.70655	0.00031	0.63758	0.00037	0.74762	0.00033
20	1.91-hex; 1.76,2.2-sq [a]	0.65976	0.00028	0.58585	0.00031	0.70517	0.00028

NOTE: *hex* is hexagonal pitch shape; *sq* is square pitch shape; [a] hexagonal pitch; [b] square pitch; maximum k_{eff} is represented in table independent of pitch shape.

The pitch shape is modeled as either a hexagonal or square pitch array (see Figure 6-Xa for pitch comparison). Table 6-37b displays k_{eff} results for a comparison of the pitch shape for the most reactive fuel rod contents, PWR_W3, for shipment with no rod container (determined in Table 6-37a). The largest variation, an increase in keff for a square pitch over hexagonal pitch, occurs when rods are tight packed. However, as the pitch is increased and/or the quantity of rods decreases then the hexagonal pitch array becomes more reactive due to optimization of the moderator-to-fuel ratio.

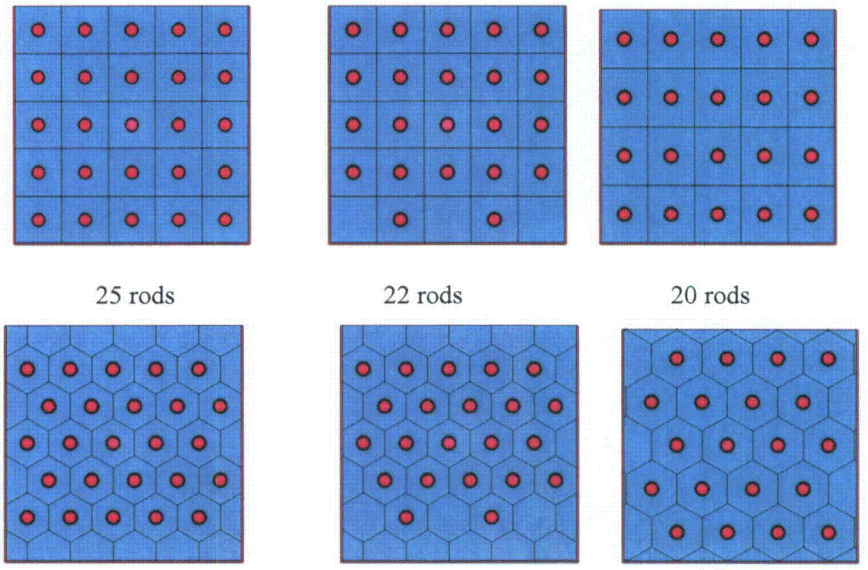

Figure Error! No text of specified style in document.**-Xa Fuel Rod without a Rod Container, Pitch Variation – Square Pitch (top) and Hexagonal Pitch (bottom)**

Table 6-37b 144 package array, No Rod Container, Pitch Shape Comparison, PWR_W3 maximum fuel category

No. of rods per IC side	Half-Pitch (cm)	Hexagonal pitch k_p	Hexagonal pitch σ_p	Square pitch k_p	Square pitch σ_p
25	Rod OR (with NPM)	0.44061	0.00031	0.45934	0.00027
25	1.3	0.7595	0.00031	0.77324	0.00034
25	1.6	0.80154	0.00034	0.79852	0.00038
25	1.60-hex; 1.76-sq	0.80154	0.00034	0.78663	0.00029
22	1.60-hex; 1.76-sq	0.74762	0.00033	0.73784	0.00033
20	1.91-hex; 1.76,2.2-sq	0.70517	0.00028	0.69094	0.00033

RAI 6-8:

Revise Section 6.6.2.2.2.1 of the SAR to clarify the assemblies selected for the criticality evaluation of inner container spacing within the outer container, as well as the contents of Table 6-40.

Table 6-40 contains information related to the keff effect of the position of the inner container within the outer container of the package. The applicant should justify the selection of assemblies used to demonstrate this effect. Additionally, it is not clear what is meant by the keffs reported for "Fuel Channel" and "Inner Container" in this evaluation.

This information is needed to ensure that the package will meet the criticality safety requirements for package arrays in 10 CFR 71.59.

Response:

Text edited in Section 6.6.2.2.2, as follows, to identify fuel assembly model used for uncertainty analyses. Additionally, SVEA fuel will be removed from Section 6.6.2.2.2.1, due to clarification of reference model, GNF2 fuel, for uncertainty in Section 6.6.2.2.2. Updates to Table 6-40 headings for uniformity in naming convention (i.e., *Fuel Assembly* and *Fuel Bundle* instead of *Fuel Channel* and *Inner Container*, respectively).

6.6.2.2.2 Geometric or Material Representations

To determine uncertainty, evaluations for geometric and material representations use the GNF2 fuel with BA rods as a reference model. This reference model, fuel with BA rods, represents the most common configuration for shipment. Additionally, the GNF2 fuel type is determined to represent the most reactive HAC package array configuration for fuel assembly and fuel bundle confinements.

6.6.2.2.2.1 Spacing within Outer Container

The rubber vibro-isolating devices are also assumed to degrade or melt when exposed to an external fire, allowing the inner container to shift downward about 2.54 cm. Maximum temperature inside the outer container is 800°C and the ignition temperature for rubber is between 260° - 316°C. The inner container horizontal position within the outer container would be the same as the normal condition model, since the stainless steel fixture assemblies remained intact following the 9-meter drop.

The effect of a shift in the position of the inner container is assessed by positioning the inner container in a corner of the outer container and evaluating k_{eff} for the infinite array. Table below demonstrates that the effect of position of the inner container within the outer container is less than 0.004 Δk_{eff} for the package array configuration.

Table 6-40 Package Array (Infinite), Spacing of Inner Container within Outer Container

Fuel Type		Confinement Boundary					
		Nominal		Fuel Assembly		Fuel Bundle	
		k_p	Δk_p	k_p	Δk_p	k_p	Δk_p
GNF2	Centered	1.13173	0.00248	1.13417	0.00272	1.13883	0.00324
	Shifted	1.13421		1.13689		1.14207	

Note: Statistical uncertainty, σ_p, in the calculation of k_p is less than 0.00030.

RAI 6-9:

Revise Figure 6-17 and associated text of the SAR to justify the selection of the GNF2 fuel assembly for the evaluation of keff due to outer container dimensional variation.

Figure 6-17 shows the variation of the hypothetical conditions of transport package array keff with changes in the spacing between the packages, for the GNF2 fuel assembly and fuel bundle. However, the associated text does not make clear why this assembly was selected for this evaluation.

This information is needed to ensure that the package will meet the criticality safety requirements for package arrays in 10 CFR 71.59.

Response:

(Similar to RAI 6-8)

Text edited in Section 6.6.2.2.2, as follows, to identify fuel assembly model used for uncertainty analyses.

6.6.2.2.2 Geometric or Material Representations

To determine uncertainty, evaluations for geometric and material representations use the GNF2 fuel with BA rods as a reference model. This reference model, fuel with BA rods, represents the most common configuration for shipment. Additionally, the GNF2 fuel type is determined to represent the most reactive HAC package array configuration for fuel assembly and fuel bundle confinements.

RAI 6-10:

Revise the application to describe how the apparent non-uniform pitch in the SVEA fuel assembly (see Figure 1-11) is accounted for in the criticality analysis, particularly with respect to the resonance self-shielding calculations performed as part of the SCALE CSAS6 calculation.

Figure 1-11 of the SAR shows that fuel rod pitch in the SVEA bundle lattice is not uniform across the assembly (see dimensions D, E, F, and G). Section 6.3.4.1.2 of the SAR describes the multiregion unit cell developed to account for redistribution of polyethylene in the package, but the criticality analysis does not describe how the unit cell is developed for the non-uniform pitch in the SVEA, or other, assembly types. The application should be revised to expand the discussion of unit cell development, specifically to include that for the SVEA assembly, but also for any other evaluation where the unit cell cannot be represented in a standard latticecell due to material or geometry considerations.

Response:

Both the multiregion and latticecell unit cell options are used to process the cross section data to account for the effects of energy self shielding and rod shadowing on resonance escape probabilities. The resonance correction techniques treat the fuel rods as a single fuel lump in an infinite moderator. To account for the heterogeneous effects of the lattice of fuel rods, a correction known as the Dancoff factor is applied to the leakage probability from the fuel rod. The algorithms in SCALE for LATTICECELL and MULTIREGION calculations are analytical methods used to determine the Dancoff factor for the fuel rods. The LATTICECELL and MULTIREGION calculations represent the fuel rod lattice in one dimension and account for the effects of neighboring fuel rods. The MULTIREGION treatment allows for a more general representation of the fuel to include an additional region of polyethylene on the outside the cladding. A white outer boundary condition is used in the unit cell description for the MULTIREGION calculation to approximate an infinite array of fuel rods. Both the LATTICECELL and MULTIREGION representations are an approximation of an infinite lattice of uniformly spaced fuel rods with negligible leakage out the ends of the fuel.

Two dimension effects of non-uniform fuel rod pitch as result of the fuel lattice design features such as partial length rods and water channels are not accounted for by the analytic methods for calculating Dancoff factors and one dimension methods used to calculate unit cell fluxes. Monte Carlo methods can be used to calculate a Dancoff factor that account two and three dimensional effects of these fuel lattice design features.

Calculation of Monte Carlo Dancoff factors is based on its collision probability definition. The program calculates the probability that a neutron emitted isotropically from the surface of the fuel region of the fuel element under consideration will have its next collision in the fuel region of any other surrounding fuel element. This probability is calculated by Monte Carlo method which is equally applicable in simple and in complicated geometries. Using the Monte Carlo method in the case of DANCOFF-MC means to select randomly the position where the neutron is emitted and the direction in which it travels. The lengths travelled in different material regions and the transport probabilities along any given path are calculated according to analytical formulae. The Dancoff factors calculated using DANCOFF-MC are applied to the unit cell calculations to account for the two dimensional rod shadowing effect for either the LATTICECELL or MULTIREGION.

Monte Carlo Dancoff factors were calculated for an infinite array of SVEA fuel bundles using DANCOFF-MC. The Dancoff factor for the uniform lattice pitch of 12.8 mm is 0.2960 as calculated by the analytic algorithm for a LATTICECELL calculation. The actual fuel rod positions and lengths were represented in a KENO-VI geometry model used to calculate the 3D Monte Carlo Dancoff factors. A summary of the Monte Carlo Dancoff factors is shown in Figure 6-X.

10	0.2974	0.2434	0.2757	0.2817	0.2270		0.2253	0.2813	0.2752	0.2405	0.2813
9	0.2655	0.2623	0.2608	0.2668	0.2061		0.2064	0.2646	0.2600	0.2581	0.2411
8	0.3021	0.2616	0.2548	0.2550	0.1850		0.1849	0.2543	0.2553	0.2600	0.2752
7	0.3109	0.2700	0.2578	0.2243	0.1598		0.1552	0.2186	0.2569	0.2682	0.2834
6	0.2546	0.2094	0.1894	0.1609				0.1578	0.1895	0.2093	0.2275
5	0.2542	0.2073	0.1847	0.1581				0.1601	0.1877	0.2093	0.2286
4	0.3097	0.2693	0.2560	0.2219	0.1585		0.1578	0.2217	0.2550	0.2687	0.2821
3	0.3034	0.2627	0.2560	0.2566	0.1854		0.1858	0.2558	0.2544	0.2610	0.2740
2	0.2658	0.2611	0.2599	0.2681	0.2081		0.2060	0.2680	0.2623	0.2608	0.2428
1	0.3150	0.2667	0.3019	0.3099	0.2530		0.2521	0.3115	0.3012	0.2671	0.2976
	1	2	3	4	5		6	7	8	9	10

Figure 6-X Monte Carlo Dancoff Factor Summary, SVEA bundle

The Dancoff values within 1 percent of reference value calculated by the analytic algorithm for a LATTICECELL are not highlighted, higher Dancoff values are highlighted in red, and lower values are highlighted in green. The lower values represent less rod shadowing and higher values more rod shadowing relative to the reference value that is 0.2690. Lower values represent physically that there is less resonance escape and have the effect of increasing the k-eff value.

The Dancoff values calculated using the Monte Carlo Dancoff method show the main effect is that of the increased moderation of the water channel. The effect of the partial length rods and non-uniform pitch within the mini-bundle quadrant are minor compared to the water channels.

The Dancoff values calculated using the Monte Carlo method were applied to the KENO-VI calculation for an infinite array of the SVEA96 fuel bundle by entering a DAN2PITCH value in the CENTRM DATA block for a LATTICECELL calculation for each fuel rod. This resulted in a lower value calculated for the neutron multiplication, k-eff, relative to approximating the rod shadowing effect, by correcting the Dancoff factors, assuming an infinite lattice of fuel rods. This result is consistent with the tendency for the Dancoff factors to be lower than those calculated using the analytic algorithm for the LATTICECELL calculation.

Dancoff Method	k-eff	σ
LATTICE CELL	1.11502	0.00024
MC-DANCOFF	1.0946	0.0030

Calculation of Dancoff factors for an isolated fuel assembly with water reflector or a fuel assembly within the packaging would result in lower values for the edge and corner rods than calculated for the infinite array of fuel bundles due to moderation near the edges of the fuel bundle.

RAI 6-11:

Revise Section 6.3.1 of the SAR to justify the replacement of wooden thermal insulator with alumina silicate in the inner container.

This section of the SAR states that wooden insulator in the inner container is replaced with alumina silicate in the criticality model configuration, but does not state why this is done. Any simplifications in the criticality model from the actual configuration should be justified to be conservative with respect to package k_{eff}.

Response:

An evaluation of packaging material configurations was done to determine the most reactive packaging configuration, see Appendix 6.9.6. The maximum neutron interaction between fuel bundles occurs when the aluminum silicate insulator material is eliminated from the inner packaging. Any moderation provided by the wooden strip for the space between the packages is accounted for by the evaluation of the effect of moderation between packages described in Section 6.6.2.2.2.3 - Moderation between Packages.

RAI 6-12:

Revise Section 6.3.1 of the application to justify the lattices used for the loose rod evaluation.

This section states which type of lattice (square or triangular) is used to evaluate loose rods in the various rod containers. The applicant should justify that the use of square lattices is conservative, considering that a triangular pitch lattice may allow for a greater mass of fissile material in the rod containers with similar rod-to-rod spacing. Note that the infinite array analysis to determine the most reactive rod in Appendix 6.9.5 is performed assuming a triangular pitch.

Response:

Note: RAI 6-7 displays the pitch type comparison for fuel rod shipments without a rod container.

Fuel rods may be transported either packaged in a rod container or as a cluster of fuel rods without a rod container. The package array with fuel rod contents is evaluated using the BWR_G3 fuel rod category, determined as the most reactive category in the infinite rod array comparison (See Appendix 6.9.5). Additionally the minimum (PWR_W5) and maximum (PWR_W3) fuel rod categories as based on fuel pellet diameter are evaluated for the fuel rod contents. Three fuel rod containers are evaluated: rod pipe, rod box, and protective case. For a rod container, the number of fuel rods is limited by the capacity of the rod container.

The package array model is used to compare pitch types, as the package array for fuel rods is a more reactive case than the individual package for fuel rods. The pitch type is first modeled to fit the container shape (i.e., square pitch in square containers and hexagonal pitch for the cylindrical container). For comparison, the other pitch option (i.e., hexagonal pitch in square containers and square pitch for the cylindrical container) was modeled for varying pitches to encompass the peak reactivity point and ±0.5 cm half-pitch. The resultant more reactive pitch type is applied to the individual package analysis.

The following tables show the pitch type comparison for the three fuel rod categories evaluated in the three fuel rod containers, respectively. Results in Table 6-Xa show for the Protective case the BWR_G3 fuel category in a square pitch type is most reactive for the NCT pitch size (rod OR) and HAC expanded pitch size at 0.80 cm. For the WEC box, as shown in Table 6-Xb, the BWR_G3 fuel category in a square pitch type is most reactive for the NCT pitch size (rod OR), while the hexagonal pitch type is more reactive for the HAC expanded pitch size at 0.80 cm. Results in Table 6-Xc for the rod pipe show a square pitch type is most reactive for the NCT pitch size (rod OR), while the hexagonal pitch type is more reactive for the HAC expanded pitch size at 0.85 cm.

For NCT, where rods are tightly packed, square pitches allow more moderator present, which in an undermoderated system increases keff. While as the pitch expands the hexagonal pitch type allows more fuel mass present in the container due to the shape and stacking-ability of the pitch type, which may increase keff. However the shape of the container has a role in the optimization of the fuel-to-moderator ratio, which along with pitch type controls the amount of fuel and moderator present.

Table 6-Xa 144 package array, Protective Case, Fuel Category and Pitch Comparison

Pitch size	Fuel Type, Pitch type (keff ±sigma)					
	BWR_G3 Square	BWR_G3 Hexagonal	PWR_W5 Square	PWR_W5 Hexagonal	PWR_W3 Square	PWR_W3 Hexagonal
Rod OR	0.49095 ±0.00024	0.43199 ±0.00027	0.48644 ±0.00029	0.43098 ±0.00023	0.46588 ±0.00027	0.41014 ±0.00022
0.65	--	--	0.59403 ±0.00031	0.58221 ±0.0003	--	--
0.70	0.60148 ±0.00034	0.58299 ±0.00032	0.60557 ±0.00029	0.59939 ±0.0003	--	--
0.75	0.60755 ±0.00033	0.60195 ±0.00031	0.59856 ±0.00032	0.60312 ±0.0003	--	--
0.80	0.61028 ±0.00031	0.60036 ±0.00032	0.58957 ±0.00032	0.5852 ±0.0003	0.58663 ±0.0003	0.57282 ±0.00032
0.85	0.60722 ±0.00033	0.59378 ±0.00033	--	--	0.59145 ±0.00035	0.57568 ±0.00036
0.90	--	--	--	--	0.58983 ±0.00037	0.58375 ±0.00032
0.95	--	--	--	--	--	0.58702 ±0.00029
1.0	--	--	--	--	--	0.58722 ±0.00034
1.10	--	--	--	--	--	0.56607 ±0.00036

Table 6-Xb 144 package array, WEC Box, Fuel Category and Pitch Comparison

Pitch size	Fuel Type, Pitch type (keff ±sigma)					
	BWR_G3 Square	BWR_G3 Hexagonal	PWR_W5 Square	PWR_W5 Hexagonal	PWR_W3 Square	PWR_W3 Hexagonal
Rod OR	0.82486 ±0.00036	0.78914 ±0.0003	0.8171 ±0.00035	0.78103 ±0.00032	0.79695 ±0.00031	0.76225 ±0.0003
0.60	--	--	0.86285	0.84842	--	--

			±0.00034	±0.0004		
0.65	--	--	0.87817 ±0.0004	0.88113 ±0.00033	--	--
0.70	--	--	0.87631 ±0.00036	0.87017 ±0.00036	--	--
0.75	--	0.87602 ±0.00035	0.8772 ±0.00041	0.86501 ±0.00034	--	0.85024 ±0.00036
0.80	0.86988 ±0.00031	0.89523 ±0.00036	0.84246 ±0.00038	--	0.85916 ±0.00033	0.8747 ±0.00037
0.85	0.87191 ±0.00039	0.87695 ±0.00036	--	--	0.86883 ±0.00033	0.86897 ±0.00039
0.90	0.8809 ±0.00039	--	--	--	0.87985 ±0.00039	--
0.95	0.82171 ±0.00041	--	--	--	0.82795 ±0.00033	--

Table 6-Xc 144 package array, Pipe, Fuel Category and Pitch Comparison

Pitch size	Fuel Type, Pitch type (keff ±sigma)					
	BWR_G3 Hexagonal	BWR_G3 Square	PWR_W5 Hexagonal	PWR_W5 Square	PWR_W3 Hexagonal	PWR_W3 Square
Rod OR	0.60923 ±0.0003	0.69781 ±0.0003	0.60941 ±0.00026	0.69466 ±0.00031	0.5802 ±0.00026	0.67183 ±0.00029
0.65	--	0.81911 ±0.00033	--	0.84252 ±0.00031	--	--
0.70	--	0.84791 ±0.00035	0.85117 ±0.00038	0.85448 ±0.00034	--	--
0.75	--	0.86077 ±0.00034	0.84822 ±0.0003	0.85105 ±0.0004	--	--
0.80	0.85776 ±0.00032	0.85384 ±0.00032	0.85001 ±0.00039	0.82955 ±0.00032	0.8205 ±0.00034	0.83357 ±0.00034
0.85	0.86587 ±0.00034	0.8486 ±0.00035	0.84757 ±0.00038	--	0.83929 ±0.00032	0.83669 ±0.0003
0.90	0.85738 ±0.00039	0.8426 ±0.00031	0.82633 ±0.00033	--	0.84296 ±0.0004	0.83933 ±0.00032
0.95	0.83027 ±0.00038	--	--	--	0.82667 ±0.00036	0.82991 ±0.00032

RAI 6-13:

Revise Section 6.3.1.3 of the SAR to clarify the modeling of the WEC rod box for shipping loose fuel rods.

This section states that the WEC rod box shell has large punched holes, which are modeled as solid in the criticality model configuration. Modeling the rod box this way may be non-conservative, as it reduces the water volume and increases parasitic neutron absorption in the steel. This section should be revised to justify that this modeling simplification is conservative.

Response:

Text changed in Section 6.3.1.1 for clarification, as follows. These model changes will affect the loose rod analysis results and updates to the summary results will be included in the SAR updates.

6.3.1.3 WEC Rod Box

Square lattices have been considered with the intent of identifying the most reactive arrangement and determining the maximum allowable number of loose rods inside the product WEC container that can be transported within the RAJ-II package. Figure 6-6 shows the SCALE model of the WEC rod box. This approach to modeling the fuel rods is conservative, since it permits the rods to be spaced in optimally moderated configurations within the cuboid and eliminates any restriction on the number of rods that can be transported in a rod container. Actual shipments will utilize the full rod container capacity such that the rods will be nearly close-packed in the rod container; however, there a partially loaded rod container is credible.

The WEC rod box is a rectangular box, composed of an external shell and internal steel bars limiting the contents spacing. The shell has large punched holes to avoid water moderation buildup within the container. Conservatively, no components of the WEC rod box are modeled, although the internal spacing is maintained and fully moderated for hypothetical accident transport conditions.

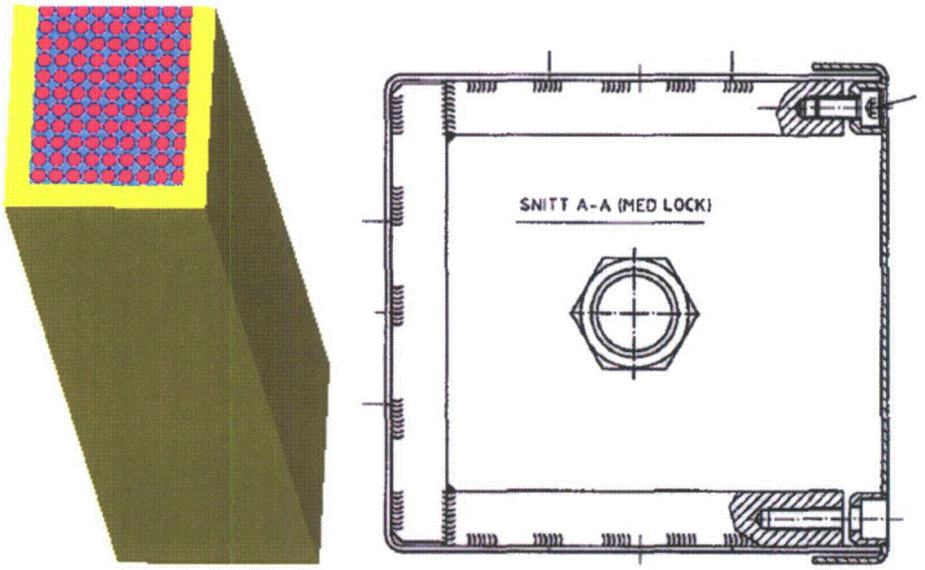

Figure 6-6 WEC Rod Box: SCALE Model slice (left), Licensing Drawing (right)

RAI 6-14:

Revise the application to clarify why the polyethylene in the criticality model configuration is represented as a mixture of actual densities, and if it is conservative to do so. Also, clarify the equation used to combine the densities, as *PI* does not appear in the equation, and both *PI* and *Pr* are listed as the density of the mixture. Additionally, clarify why a volume weighted density is used for the normal conditions of transport model, while the standard material density is used for hypothetical accident conditions, and how this modeling approach is conservative. Lastly, revise the application to state the maximum mass of polyethylene that may be present in the package, and ensure that this maximum mass is considered in the criticality analysis.

The representation of polyethylene in the criticality model configuration can have a large impact on calculated keff due to its potential to have a higher hydrogen density than water. For this reason, it is important that the representation of polyethylene is adequately described in the criticality analysis.

Response:

Discuss of the polyethylene densities and use is clarified, as follows.

See RAI 6-34 regarding the discussion of polyethylene modeling and melting phase reactivity.

6.3.2.5 Polyethylene

Standard material POLY(H2O) is used to represent all polyethylene packing and packaging materials in normal and accident transport conditions (plastic sheathing, foam cushions, and melted foam). The POLY(H2O) composition is CH_2, density is 0.92 g/cc, and uses hydrogen in the water S(α,β) thermal kernel.

The densities of the polyethylene materials are as follows,

Cluster separator fingers (LDPE)	0.925 g/cm^3
Cluster separator holders (HDPE)	0.959 g/cm^3
Protective sheath	0.919 g/cm^3
Foam cushion	0.080 g/cm^3

Where polyethylene material is represented by a mixture of the components (i.e., cluster separator assembly units), the following equation are used to calculate the weighted average density:

$$\frac{1}{\rho_T} = \sum_i \frac{\omega_i}{\rho_i} \text{ where,}$$

ω_i is the weight fraction of material/component i,

ρ_i is the density of the material/component i, and

ρ_T is the density of the mixture.

Instead of representing the actual material distribution within the contents, an equivalent mass of material is distributed uniformly around each of the fuel rods as a wrap. The uniform poly wrap on each rod is conservative, as compared to several melting stages of the polyethylene for HAC; any positive reactivity from melting stages based on transport condition is included as additional uncertainty to k_u. (See RAI 6-34)

6.3.2.5.1 Cluster Separator and Protective Sheath

When fuel assemblies are shipped without a channel as a fuel bundle, polyethylene inserts or polyethylene cluster separators are positioned between fuel rods at various locations along the axis of the fuel assembly to avoid stressing the axial grids during transportation. The cluster separators are shown in Figure 6-1 provide a higher volume average density polyethylene inventory, hence are chosen for the RAJ-II criticality analysis. The cluster separator is composed of Low Density Polyethylene (LDPE, 0.925 g/ cm^3) fingers and a High Density Polyethylene (HDPE, 0.959 g/ cm^3) holder. For a 10x10 cluster separator assembly unit, the LDPE fingers occupy an approximate volume of 38 cm^3 while the HDPE holder has an approximate volume of 85 cm^3. A weight average density of 0.949 g/cm^3 is calculated for the polyethylene cluster assembly as a mixture of the actual densities since the cluster separator assembly is modeled as a single unit. The calculation is as follows:

$$\omega_{LDPE} = \frac{V_{LPDE}\rho_{LPDE}}{V_{LPDE}\rho_{LPDE} + V_{HPDE}\rho_{HPDE}} = \frac{38cm^3 \times 0.925 g/cm^3}{38cm^3 \times 0.925 g/cm^3 + 85cm^3 \times 0.959 g/cm^3} = 0.30$$

$$\omega_{HDPE} = 1 - \omega_{LDPE} = 1 - 0.30 = 0.70$$

$$\frac{1}{\rho_T} = \frac{\omega_{LDPE}}{\rho_{LDPE}} + \frac{\omega_{HDPE}}{\rho_{HDPE}} = \frac{0.30}{0.925} + \frac{0.70}{0.959} = 1.054$$

$$\rho_T = 0.949 g/cm^3$$

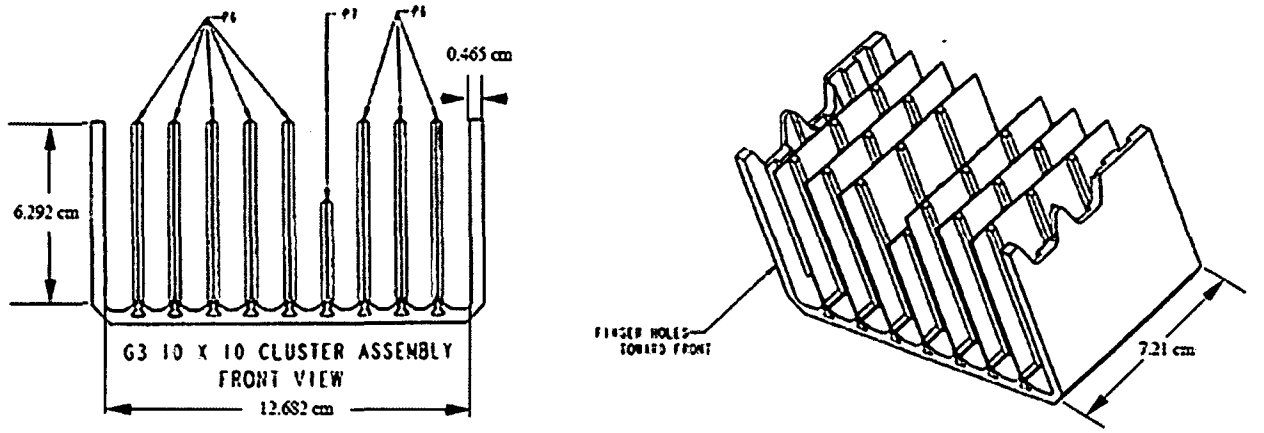

Figure 6-1 Polyethylene Cluster Separator

The fuel bundle and fuel assembly is also wrapped in a polyethylene protective sheathing. The mass of sheath varies with the fuel design, within the range of 582 g to 672 g, based on a 10 mil bag wrapped around the assembly with a length of the assembly plus 12 in.

The cluster separator assembly and protective sheath make up the normal packing materials, and are conservatively modeled as a uniform polyethylene wrap around each rod in the bundle. Modeled as a single material wrapped around each rod, a weight average density of 0.947 g/cm^3 is calculated for the polyethylene material as a mixture of the actual densities. Additional

information provided in Section 6.3.4.1.2. The calculation for the polyethylene normal packing materials density is below. The poly wrap composed of normal packing materials is present for NCT and HAC models, as conservative modeling of polyethylene presence.

Fuel assemblies do not utilize cluster separators as they are channeled, hence only the protective sheath bag at its nominal density (0.919 g/cm^3) is modeled as a uniform wrap around each rod.

$$\omega_{CLUSTER\,SEP} = \frac{V_{CLUSTER\,SEP}\rho_{CLUSTER\,SEP}}{V_{CLUSTER\,SEP}\rho_{CLUSTER\,SEP} + V_{SHEATH}\rho_{SHEATH}} = \frac{8000\,cm^3 \times 0.949\,g/cm^3}{8000\,cm^3 \times 0.949\,g/cm^3 + 700\,cm^3 \times 0.919\,g/cm^3} = 0.92$$

$$\omega_{SHEATH} = 1 - \omega_{CLUSTER\,SEP} = 1 - 0.93 = 0.08$$

$$\frac{1}{\rho_T} = \frac{\omega_{CLUSTER\,SEP}}{\rho_{CLUSTER\,SEP}} + \frac{\omega_{SHEATH}}{\rho_{SHEATH}} = \frac{0.92}{0.949} + \frac{0.08}{0.919} = 1.056$$

$$\rho_T = 0.947\,g/cm^3$$

The evaluation of polyethylene in the package sets limits for the total polyethylene mass based on the component and its corresponding maximum average density as shown in Table 6-X. Other types of inserts or polyethylene packing materials are acceptable provided that their polyethylene inventory is within the limits established using the cluster separators and sheathing bag.

Table 6 Error! No text of specified style in document.**-X Polyethylene Mass and Density Limits**

Material	Mass (kg)	Maximum Volume Weighted Density
Ethafoam packaging/packing	11.21	0.08 g/cm^3
Polyethylene packing (i.e. sheathing bag & cluster separators)		
GNF Fuels	8.11	0.947 g/cm^3
WEC Fuels (SVEA only)	0.65	0.919 g/cm^3

RAI 6-15:

Revise the SAR to provide documentation of the approach used for the TSUNAMI-3D calculations, particularly any confirmatory direct perturbation calculations that have been performed.

...

Response:

Calculation Note, *CN-LCPT-10-2, BA Rod Worth Evaluation of BWR Fuel Designs for Shipment in RAJ-II Package*, included for additional information of full TSUNAMI-3D review. This full analysis is referenced in the SAR, however, detailed evaluation not to be included directly into the SAR.

RAI 6-16:

Revise the application to provide representative input and output files for key TSUNAMI calculations.

NUREG-1609, *Standard Review Plan for Transportation Packages for Radioactive Material,* recommends that, for computer codes used in the criticality analysis, at least one representative output file (or key sections) should be included in the application.

Response:

All input and output files have been included on CD previously sent to NRC for review. This method has been discussed and approved by NRC staff.

RAI 6-17:

Revise Table 6-9 of the SAR to provide the number of histories per generation and convergence criteria (SIG value), if used.

This table provides relevant information regarding the SCALE CSAS6 code parameters used in the criticality evaluation, but does not provide the total number of histories per generation, or the convergence criteria.

Response:

Additional parameters and settings added to Table 6-9 for clarification, as follows:

Table 6-9 CSAS6 Parameter Values

Parameter	Value for KENO in CSAS Sequences or as stand-alone code	Description
CFX	NO (default)	collect fluxes
GEN	550	number of generations to be run
NSK	3 (default)	number of generations to be omitted when collecting results
NPG	10000	number of particles per generation
PNM	0 (default)	highest order of flux moments tallies
SIG	0 (default)	deviation limit
TFM	NO (default)	perform coordinate transform for flux moment and angular flux calculations

RAI 6-18:

Revise Table 6-10 of the SAR to provide the number of histories per generation and the adjoint convergence criteria (ASG value), if used. Additionally, provide the spatial meshing strategies and direct perturbation approach used in the TSUNAMI evaluation.

This table provides relevant information regarding the SCALE TSUNAMI code parameters used in the criticality evaluation, but does not provide the total number of histories per generation, or the adjoint convergence criteria.

Response:

Additional parameters and settings added to Table 6-10 for clarification, as follows:

Table 6-10 TSUNAMI Parameter Values

Parameter	Value for TSUNAMI-3D	Corresponding KENO parameter	Description
ABK	APG × 2	NBK = NPG+25 (default)	number of positions in the neutron bank for the adjoint calculation
AGN	GEN = NSK + ASK	GEN = 203 (default)	number of generations to be run for the adjoint calculation-default value produces the same number of active generations as the forward calculation
APG	NPG × 3	NPG = 10000	number of particles per generation
ASG	SIG (default SIG = 0)	SIG	if > 0.0, this is the standard deviation at which the adjoint problem will terminate
ASK	NSK × 3	NSK = 3 (default)	Number of generations to be omitted when collecting results for the adjoint calculation

RAI 6-19:

Revise Section 6.3.3.3 of the SAR to provide sample direct perturbations used to verify the validity of the uncertainty evaluation approach for material and fabrication tolerances.

...

RAI 6-20:

Revise Section 6.3.3.3 of the SAR to provide a parametric evaluation comparing direct calculations to TSUNAMI results for the uncertainty evaluation for material and fabrication tolerances.

...

RAI 6-21:

Revise Section 6.3.3.3 of the SAR to remove the assertion that simple summation of individual relative uncertainties provides conservatism in the analysis.

...

RAI 6-22:

Revise Section 6.3.3.3 of the SAR to justify the validity of the assumption that $\Delta keff/keff$ is independent of the absolute value of k_P.

...

Response to RAIs 6-19, 6-20, 6-21, 6-22:

The uncertainty analysis has been reevaluated using a standard direct perturbation approach; hence Section 6.3.3.3 will be completely removed and a new section will include the following discussion.

6.x Uncertainty Evaluation for Material and Fabrication Tolerances

For the tolerance values being studied in this system, the reactivity affect on the system must be determined based on a change in the total amount of the material of interest present. This can be accomplished by the study of an explicit change in material volume due to tolerance value. Tolerances for each parameter evaluated are displayed in Table 6-X.

Direct perturbations of each parameter are calculated individually to determine the conservative uncertainty for a particular parameter tolerance. Any positive reactivity from the parameter variation is added to the total uncertainty Δk_u. The total absolute uncertainty, Δk_u, is the combined uncertainty of material tolerances and material and geometric representation evaluations.

The individual uncertainties are aggregated as a simple sum instead of combining using a statistical sum such as root mean square. This results in a conservative estimate of the uncertainty as the simple sum ignores the possibility that the material tolerances are dependent of each other.

Table 6-X Tolerance Specifications

Parameter	Tolerance	Reference
Fuel pellet diameter	0.20%	AA 284999 [6]
Clad thickness (fuel tube)	1%	AA 294145 [7]
Fuel rod pitch (fuel bundle water moderator)	1%	AA273878 [8]
Packaging steel sheet	10%	ASTM A480 / A480M-10
Polyethylene (annulus around fuel rod)	1%	Note 1

Note 1 - There is no reference for the uncertainty in the quantity of polyethylene available in the packaging. The polyethylene thickness is assumed to vary the same as the clad thickness.

RAI 6-23:

Revise Section 6.3.4.1.1 to demonstrate that spatial self-shielding effects are not important when using a small amount of Gd_2O_3 to assess sensitivity for the actual Gd_2O_3 content in the system.

As more Gd_2O_3 is added, it is possible that the sensitivity decreases due to decreased effectiveness of Gd_2O_3 at the center of the pin, which is shielded by the increased density of Gd_2O_3 at the edge of the pin. A parametric evaluation of 157Gd sensitivity as a function Gd_2O_3 density would clarify this issue.

Response:

For evaluation of most reactive BA rod positions, each available BA rod position is doped with 0.1% Gd_2O_3, represented in the material composition as 0.1% volume fraction of UO_2 theoretical density 10.96 g/cm^3. The presence of the Gd_2O_3 is minimal, hence not impacting the flux profile characteristics.

A new evaluation was conducted to investigate the impact of Gd_2O_3 density (wt%) on the ^{157}Gd sensitivity used to evaluate relative worth of viable BA rod positions within the assembly. The Gad volume fraction was varied, and the sensitivity coefficients of ^{157}Gd were compared. Gad volume fraction of fuel evaluated includes 0.001, 0.01, 0.05, 0.1, 0.5, 1.0, and 2.0%.

Figure 6-X shows the ^{157}Gd sensitivity per assembly location for each evaluated Gd_2O_3 volume fraction. For an increase in the sensitivity of ^{157}Gd (S_k), the amount of Gd_2O_3 present does not consistently increase or decreases. However, it is noted that similar relative worth is seen for each rod position, while at 0.1% the relative worth of each rod position is more pronounced between positions and is the largest sensitivity between 0.001% and 2% Gd_2O_3 density. The increase or decrease in Gd_2O_3 density from 0.1% results in a damping of the relative worth by either suppression of the system by over absorption or lack of presence of Gd_2O_3 absorption, respectively.

Lower Gd_2O_3 presence allows for less absorption and a higher system reactivity. While an increased presence of Gd_2O_3 may cause more absorptions at the rim or edge of the rod due to self-shielding, this effect is not a concern for fresh fuel; whereas with irradiation there is increased fission density at the edge of the pin that affects local power.

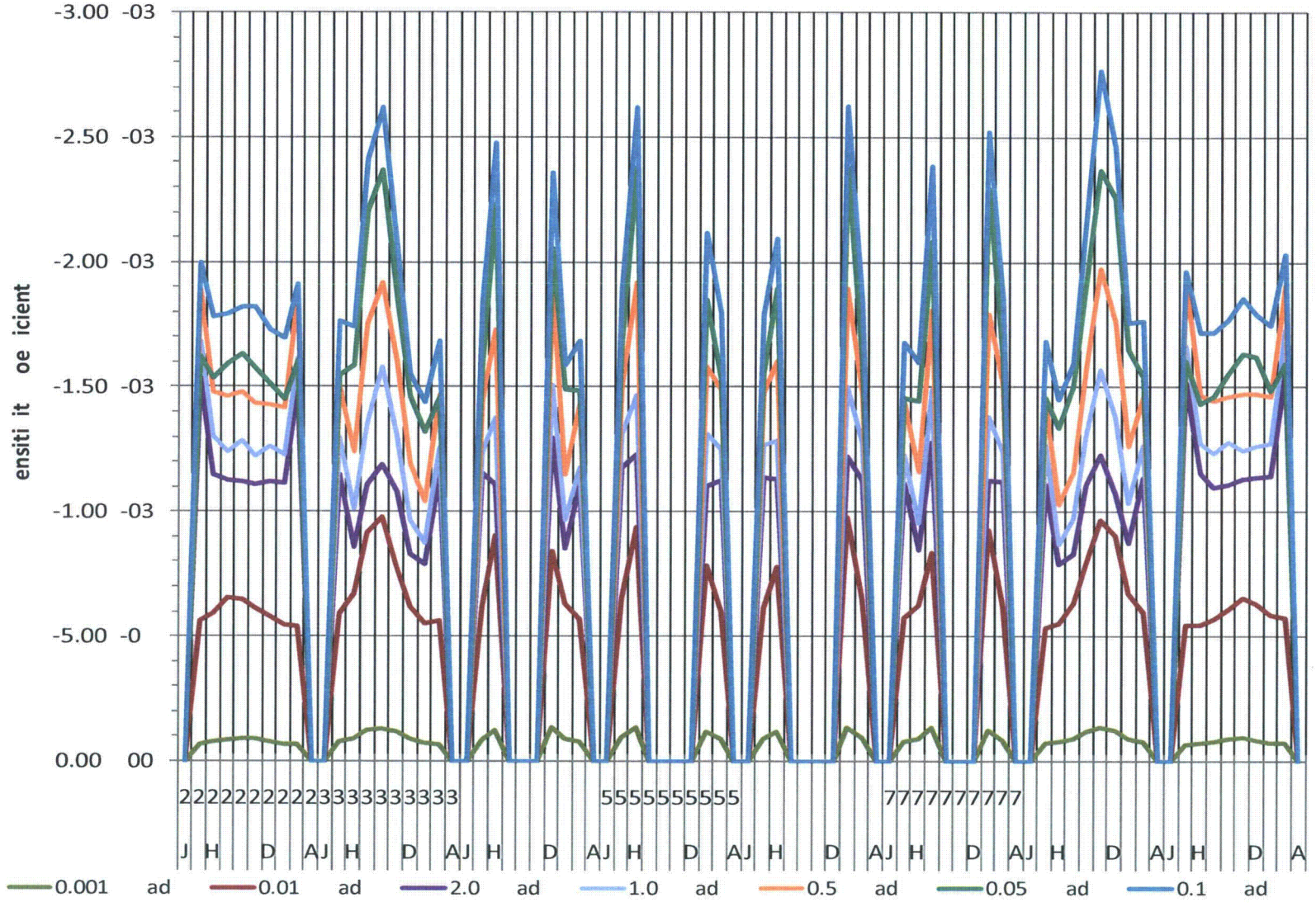

Figure 6-X GNF2 Gad Density Comparison by Assembly Position

RAI 6-24:

Revise Section 6.3.4.1.2 of the SAR to demonstrate how the moderator radius is defined in the cylindrical multiregion unit cell used to correct for resonance self-shielding. Additionally, clarify if this unit cell is used only in the lattice pitch expansion evaluation, or whenever polyethylene packing materials are assumed to be in the lattice.

On p 6-39 of the SAR, the applicant states that "the effect of polyethylene packing materials on resonance self shielding is accounted for in the cross-section processing by specifying a cylindrical multiregion unit cell as shown in Figure 6-13." This section should be revised to clarify if a uniform lattice is considered, and how the radius is corrected to preserve the Dancoff factor. Also, although this discussion appears in the lattice expansion section of the analysis, it appears that this unit cell approximation would be necessary any time there is polyethylene in the lattice, which also occurs in the unexpanded lattice. The applicant should clarify if this approach is used for resonance self-shielding calculations elsewhere in the analysis, and if not, what approach is used.

Response:

Text changed in Section 6.3.1.1 for clarification, as follows:

6.3.4.1.2 Lattice Expansion

...

In addition to the geometry representation in the model, the effect of polyethylene packing materials on resonance self shielding is accounted for in the cross-section processing by specifying a cylindrical multiregion unit cell as shown in Figure 6-13. The lattice effects are approximated by applying a white boundary condition to the cylindrical multiregion unit to represent a uniform lattice. Although the geometric lattice cell may be hexagonal or square, the moderator region is converted to a cylindrical geometry for cross-section processing by the multiregion unit celldata. The moderator cylindrical radius is calculated preserving area by setting the moderator lattice cell area (i.e., square or hexagonal region) equal to the cylindrical area and solving for the radius (MODR). Conversion equations are shown below for a square and hexagonal geometry, respectively:

$$\pi R^2 = P^2$$

$$\pi R^2 = 2\sqrt{3}(P/2)^2$$

where,

R is the radius of the equivalent circle (MODR)

P is the pitch of the cell (i.e., square or hexagonal)

This technique is always applied when polyethylene packaging materials are present to ensure the additional hydrogen content is accounted for in the cross-section processing of the model. Therefore, the NCT and HAC model utilizes the maximum allowable polyethylene mass of normal packing materials and applies it uniformly over the full axial length of the fuel.

The results for the lattice expansion evaluation are in Appendix 6.9.4.

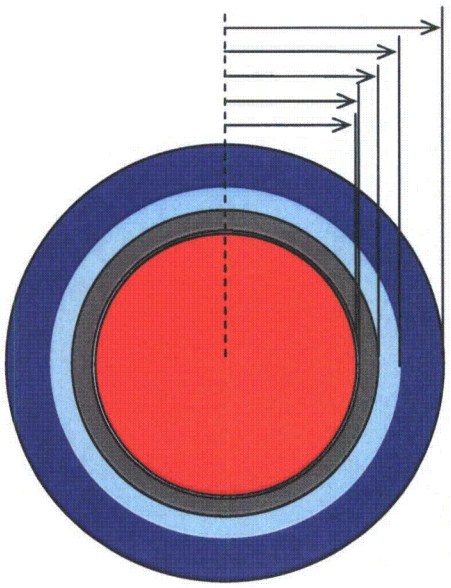

CELLTYPE CS RIGHT_BDY FUELR GAPR CLADR POLYR MODR

multiregion cylindrical right_bdy=white end 1 0.444 0 0.453 3 0.513 21 0.5888 4 0.7306 end zone

Figure 6-2 SCALE Unit Cell Demonstration for Re-distribution of Polyethylene

RAI 6-25:

Revise the criticality analysis to clarify how resonance self-shielding calculations were performed for various axial regions of the fuel assembly with and without partial length fuel rods.

The SAR does not discuss how resonance self-shielding calculations were performed for axial sections of the fuel assembly which may have fewer rods due to the inclusion of short and long partial length fuel rods. The effect of the partial length rods is to remove fuel and add moderator to the lattice, requiring a correction to the self-shielding calculations in these regions to account for more moderator. The criticality analysis should be revised to contain a comprehensive discussion of resonance self-shielding evaluations for the varying number of rods in different axial segments of the assembly, as well as for different moderation conditions (i.e., polyethylene versus water).

Response:

The effect of the partial length rods on self shielding calculations is included in the response to RAI 6-10. A 3D Monte Carlo calculation of dancoff factors was used to evaluate both the combined effect of non-uniform pitch and partial length rods. The effect of introducing moderator in the lattice zones where the partial length rods vanish is minor relative to the including the effect of the water channel in the calculation of Dancoff factors to account for rod shadowing effects.

RAI 6-26:

Revise Section 6.3.4.1.3 of the SAR to clarify the selection of fuel assemblies for the criticality evaluation with and without BA rods.

Although the evaluation discusses the key differences between several classes of fuel assemblies, it is unclear why the GE14C and GE14G assemblies were chosen for the evaluations with and without BA rods, respectively, and what the difference is between these assembly designs.

Response:

6.3.4.1.3 Summary of Most Reactive Configuration for Contents Fuel Bundle or Fuel Assembly

Structural features of the fuel bundle (grids, tie plates, handle) are considered to limit the lattice expansion, but only materials in the active length of the fuel rod (fuel pellet and cladding) are considered in the evaluation of reactivity. The other fuel bundle components are fabricated from materials (stainless steel, inconnel, and zircalloy) that absorb neutrons by radiative capture or volume of the structure displaces moderator in the fuel lattice. Representing the fuel bundle components as water results in an increase in reactivity due to both a decrease in neutron absorption and increase in fuel rod lattice moderation. Partial length rods are a feature of the fuel bundle design, and as such are considered in the demonstration of the most reactive configuration.

The most reactive configuration for the fuel bundle and fuel assembly takes into consideration the Gd_2O_3 content in the BA rods, position of neutron absorbing BA rods in the fuel bundle, position of partial length rods, moderation by packing materials and lattice expansion as result of fuel bundle rearrangement during accident transport conditions.

The fuel rod lattice moderation is less than optimum for the extent of lattice expansion that is considered as limited by the confinement system. The 10X10 fuel lattice is the most reactive configuration for the fuel bundle within the range of fuel rod pitch limited by the confinement system for lattice expansion within a maximum credible fuel length of 50 cm. Lattice expansion is uniform along a 50 cm axial length at one end of the fuel bundle. The maximum lattice pitch is a value that depends on the condition of transport and confinement boundary. The lattice pitch for an undamaged package is the nominal fuel rod pitch. For a damaged package the maximum fuel rod pitch is limited to the fuel channel for a fuel assembly or the inner container for a fuel bundle.

Although the reactivity of the 10X10 fuel bundle configurations are similar, three of the fuel bundle configurations that represent design differences are used in the package evaluation. These differences are characterized by partial length rod and water rod arrangements as follows:

GE14 is a GNF fuel design with only long partial length rods and central water rods.

GNF2 is a GNF fuel design with long and short partial length rods and central water rods.

SVEA is a Westinghouse fuel design with water cross and central water channel.

The GE14G, GNF2, and SVEA fuel bundle configurations are used for the evaluations without BA rods (i.e., individual package and small array sizes) and GE14C, GNF2, and SVEA fuel bundle configurations are used for the evaluations with BA rods (i.e., large array sizes). The selection of these fuels is based on the bundle lattice expansion comparison in Appendix 6.9.4; the fuels represent the most reactive fuel designs at nominal and peak reactivity for expanded lattice pitches.

...

RAI 6-27:

Revise Section 6.3.4.2 of the application to clarify the spacing of fuel assemblies in the inner container under hypothetical accident conditions.

On p 6-43 of the criticality analysis, the applicant states that the "polyethylene foam cushion, represented as region 2 for normal transport conditions, may redistribute from region 2 to the fuel bundle due to melting at elevated temperature during a fire event." Although this situation would allow for the two fuel assemblies to move closer together in the inner container, it is unclear if this situation has been evaluated in the criticality analysis.

Response:

New section added (6.6.2.2.2.4 Orientation in Inner Container) to account for uncertainty of the fuel assembly orientation in the inner container.

6.6.2.2.2.4. Orientation in Inner Container

The ethafoam cushioning within the IC is assumed to degrade or melt when exposed to an external fire, allowing the assembly to shift within the inner container. A following drop, may also allow the assembly to shift within the inner container.

The effect of orientation of the fuel within the inner container is assessed by positioning the fuel in the four corners of the inner container and evaluating *keff* for the infinite array, independently. Table 6-X below demonstrates that the effect of orientation of the fuel within the inner container is less than 0.015 Δk_{eff} for the package array configuration.

Table 6-X Package Array (GNF2) w/ BA rods, Orientation in IC

Confinement Boundary	Fuel Assembly			Fuel Bundle		
Position	k_p	σ_p	Δk_p	k_p	σ_p	Δk_p
center	0.86997	0.0003	0	0.90647	0.00035	0
outer-bottom	0.86459	0.00034	-0.00530	0.90252	0.00037	-0.00273
inner-bottom	0.88377	0.00038	0.01396	0.91336	0.00034	0.00481
outer-top	0.86415	0.00034	-0.00574	0.90314	0.0035	-0.00219
inner-top	0.88412	0.00033	0.01421	0.91307	0.00036	0.00523

RAI 6-28:

Revise Sections 6.4.2.2, 6.5.2.2, and 6.6.2.2 of the SAR to clarify for which package configurations the material and fabrication tolerance uncertainty evaluations are performed.

These sections state that material and fabrication tolerance uncertainty evaluations are performed, and provide tables containing the results of these evaluations. It is unclear, however, which configuration in each section these analyses are performed for (i.e., fuel assemblies, bundles, or rods). These sections should be revised to adequately describe the evaluated configuration, and justify why each configuration was chosen for the evaluation.

Response:

Uncertainty analysis is provided for the individual package and package array with and without BA rods. Uncertainties are represented by material and fabrication tolerances and geometric or material representations in the models. The combination of these uncertainties represents the total uncertainty, Δk_u, for the individual or package array analysis. Models chosen for uncertainty analyses represent the most reactive contents configuration for the package analysis, whether individual or package array.

Uncertainty values are the sum of positive reactivity changes from variations of material and fabrication tolerances and geometric or material representations. The uncertainty values represent the difference of $k_p + 2\sigma_p$ for the configuration as compared to the representative package case used for determining the most reactive case per transport condition.

The individual package uncertainty analysis is evaluated using the GNF2 and GE14C fuel models. The NCT uncertainties are the material and fabrication tolerances. The HAC uncertainty evaluation accounts for shifting components and package material effects, as well as material and fabrication tolerances. Per uncertainty parameter, only the largest positive reactivity is added to the uncertainty total.

For the package array case, the uncertainty contributors are the same for fuels evaluated with and without BA rods. The GNF2 fuel is used as the reference model for uncertainty evaluations, as it represent the most reactive HAC package array configuration. For NCT, the material and fabrication tolerances are the only uncertainties. While for HAC, uncertainties include shifting components including the packages in the array and within the package, package material effects, and material and fabrication tolerances. Per uncertainty parameter, only the largest positive reactivity is added to the uncertainty total.

Table 6-X Uncertainties for Package Models

Parameter	NCT w/o BA	HAC w/o BA	NCT w/ BA	HAC w/ BA	NCT w/o BA	HAC w/o BA
Package lattice size	package array nominal	package array Exp-IC	package array nominal	package array Exp-IC	individual package nominal	individual package Exp-IC
assembly shift in IC	--	0.00547	--	0.00523	--	0.00123
IC shift in OC	--	0.0039	--	0.00322	--	0
container deformation	--	0.00252	--	0.00266	--	--
polyethylene modeling	0.01807	0.02713	0.01807	0.02713	0.01807	0.02713
Manufacturing Tolerances						
Fuel pellet diameter	0.00102	0.00036	0.00042	0.00074	0.00087	0.00039
Clad thickness	0.01455	0.00194	0.01045	0.00199	0.00403	0.00149
Fuel rod pitch	0.00077	0.00249	0.00070	0.00100	0.00642	0.00024
Material Tolerance						
Packaging steel	0.0144	0.01051	0.01286	0.00933	0.00258	0.0021
Polyethylene (annulus on fuel rod)	0.01775	0.00025	0.01259	0.00022	0.00129	0.00093
Total Uncertainty, Δk_u	0.067	0.055	0.055	0.052	0.033	0.034

NOTE: *Exp-IC* means expanded lattice to the inner container, fuel bundle model;

RAI 6-29:

Revise Table 6-22 of the SAR, and any similar table in the evaluation (e.g., 6-29, 6-38, 6-39) to include statistical uncertainties in the sensitivity coefficients from the Monte Carlo calculations.

The referenced tables provide the results of the applicant's uncertainty evaluation for material and fabrication tolerances, and include relevant sensitivity and keff information from the analysis. Missing from these tables are the statistical uncertainties in the sensitivity coefficients from the Monte Carlo calculations performed as part of this analysis. These tables should be revised to provide this information.

Response:

The uncertainty analysis has been reevaluated using a standard direct perturbation approach; therefore the referenced tables have been removed. However, all statistical uncertainties from the Monte Carlo calculations have added or included.

RAI 6-30:

Revise Section 6.8.2 of the SAR to provide the results of the normality tests to ensure the applicability of the statistical approach for the selected benchmarking data set.

For USLSTATS analysis, the results of the normality tests, whether those from USLSTATS or other statistical packages, need to be provided to ensure applicability of statistical approach for the selected data set. Additionally, the sufficiency of applicable benchmarks should be discussed, especially for Figure 6-23 where only 9 data points are shown.

Response:

A revised method has been selected in order to properly account for the limited number of benchmarks used in the Upper Safety Limit (USL) analysis. This method is based on the non-parametric statistical treatment presented in NUREG/CR-6698, which provides the following formula for determining a USL:

$USL = K_L - \Delta_{SM} - \Delta_{AOA}$

K_L : Single Sided Lower Tolerance Limit

Δ_{SM} : Minimum Subcritical Margin

Δ_{AOA} : Area of Applicability Margin

The first step in the revised method is to use USLSTATS to determine the applicability of the selected benchmark cases to the specific arrays of RAJ-II packages being studied. Any benchmarks which result in a correlation value (c_k) below 0.80 are removed from consideration.

Next, a degree of confidence is calculated, based on the desired population fraction of 0.95, or 95%. This takes the form of the following equation, provided as Equation 32 in NUGREG/CR-6698:

$\beta = 1 - q^n = 1 - 0.95^n$

β : Degree of Confidence

q : Desired Population Fraction

n : Number of Data in One Sample

β is then used to determine the Non-Parametric Margin, in accordance to the NUREG. This margin varies between 0.01 and 0.05.

From this, K_L can be determined as:

K_L = Smallest k_{eff} value – Uncertainty for Smallest k_{eff} – Non-Parametric Margin

This is inserted into the USL equation provided above, from which the USL for any given package array can be determined, properly accounting for the possible lack of normalcy provided by small benchmark populations.

RAI 6-31:

Revise Appendix 6.9.3 of the SAR to provide direct calculations to demonstrate the validity of the TSUNAMI data for the BA rod worth evaluation.

The sensitivity of keff to the 157Gd cross section is not necessarily equivalent to its worth in terms of reactivity. As noted earlier, the TSUNAMI sensitivity coefficients are based on first-order linear perturbation theory. The reactivity effect of removing a BA rod is likely a non-linear effect. Direct calculations should be performed and documented to demonstrate the validity of the TSUNAMI data for the intended application.

Response:

(Same as RAI 6-15)

Calculation Note, *CN-LCPT-10-2, BA Rod Worth Evaluation of BWR Fuel Designs for Shipment in RAJ-II Package*, included for additional information of full TSUNAMI-3D review. This full analysis is referenced in the SAR, however, detailed evaluation not to be included directly into the SAR.

RAI 6-32:

Revise Appendix 6.9.3 of the SAR to provide keff or k_{inf} calculations to demonstrate that the BA rod pattern resulting from the BA rod worth evaluation is more reactive than other typical BA rod patterns.

The applicant provides a thorough summary of the BA rod worth sensitivity calculations performed to generate most reactive BA rod patterns for each assembly type in Appendix 6.9.3. This evaluation should be revised to include representative keff or k_{inf} calculations to provide reasonable assurance that the resulting BA rod patterns are in fact the most reactive.

Response:

(Same as RAI 6-15, 6-31)

Calculation Note, *CN-LCPT-10-2, BA Rod Worth Evaluation of BWR Fuel Designs for Shipment in RAJ-II Package*, included for additional information of full TSUNAMI-3D review. This full analysis is referenced in the SAR, however, detailed evaluation not to be included directly into the SAR.

RAI 6-33:

Revise Appendix 6.9.4 of the SAR to justify the assertion that the sensitivity to changes in lattice pitch is greater for an individual package configuration than for the package array configuration.

This section states that this assertion is valid due to the limited lattice expansion assumed in the analysis, which would affect the individual package evaluation more so than an array evaluation due to the relative fraction of fissions in the water reflected system versus the array. It is not clear from the discussion in this paragraph on p 6-97 that this assertion is true. This section should be revised to provide the results of analyses that demonstrate that the effect of lattice expansion is larger in the individual package than in the package array.

Response:

6.9.4 Fuel Bundle Lattice Expansion Evaluation

The effect on k_{eff} of increasing the lattice pitch in the fuel bundle is evaluated for a configuration that represents the individual package and package array. The effect is evaluated with and without the normal packing materials. The individual package evaluation is done without BA rods where as the package array evaluation is done with BA rods.

The sensitivity of k_{eff} to changes in lattice pitch is greater for an individual package configuration than for the package array configuration. As the system changes from full leakage in the individual package to no leakage in the infinite page array, the variation in keff becomes less pronounced or has smaller sensitivity over the same range of pitch sizes. As shown in comparing Figures 6-33 and 6-35 or Figures 6-34 and 6-36 for systems with normal packing materials. In addition to the lattice pitch expansion, the difference in sensitivity is also due to the confinement of the lattice expansion to a 50 cm axial length. For the individual package configuration, the expanded lattice accounts for a major portion of the fissions occurring in a fully water reflected system. In the package array configuration, k_{eff} is influenced by the neutron interaction between fuel bundles, where about one fourth of the length is an expanded lattice and the remainder is at nominal pitch.

RAI 6-34:

Revise the SAR to discuss the possible relocation of polyethylene packing material into higher density regions under both normal conditions of transport and hypothetical accident conditions. Additionally, discuss how the additional polyethylene packing material recommended to be used for packing loose rods in Section 7.0 of the SAR, with or without a rod container, is accounted for in the criticality analysis.

Given that there are no controls on how the polyethylene packing material is placed in the package, it would be reasonable to assume that the same impact that might produce lattice expansion in one end of the assembly, would also tend to concentrate polyethylene packing material in that same region. The criticality analysis as described assumes that the polyethylene packing material will be uniformly distributed throughout the package contents, which may not be the case under either normal conditions of transport or hypothetical accident conditions. Additionally, several sections of the package operating procedures give the option of including additional polyethylene packing material when packing loose rods, either with or without a rod container. This potential for additional moderating material should be considered in the criticality analysis.

Response:

When the fuel assembly is packed into the packaging, the packing material such as cluster separators made of polyethylene, polytheylene bags, and ethafoam cushioning are used. An evaluation of such materials on the criticality analysis is conducted. The calculation is performed for melting material variations for an arrayed system of damaged packages.

As a result of the fire test of the RAJ-II package, the melting of the fuel assembly packing materials and the cushioning materials within the inner container had been observed (Ref. Japanese SAR). Inspection of the contents after cooling, melting of the polyethylene parts and attachment of the molten polyehtylene on the dummy fuel rods was observed (Ref. Japanese SAR).

The criticality analysis models are established to follow the melting progress of the polyethylene parts in accordance with temperature rising under the fire test conditions. The process of melting and moving of the polyethylene parts is categorized by two melting stages and one normal stage. For each melting stage, two cases are evaluated representing horizontal and vertical placement of the package. The outside region from the internal wall of the inner container is the same model for each stage.

For an undamaged package model, the polyethylene materials are assumed to be in original shapes and positions. Therefore Stage 1 represents a before melting state where the normal packing materials are inserted between each row of rods and ethafoam cushioning material is positioned on the IC walls.

As for the damaged package model, several cases are evaluated following the polyethylene material variations as a fire may continually melt the material with progressing presence. The volume of polyethylene to be melted or wrapped on rods is evaluated in two stages. Stage 2 represents an intermediate melting phase, where only the ethafoam cushioning material around the assembly in the IC is fully melted. Stage 3 represents full melt, where all polyethylene materials in the IC including ethafoam cushioning and normal packing materials are fully melted. Based on stage, the volume of melted polyethylene is calculated, defined at the weighted packing material density of 0.947 g/cm^3. The volume of polyethylene to melt is smeared over the defined IC space (minus the occupying rod space), fully filling a uniform level in the IC.

Base case for comparison represents the most reactive, damaged package array for HAC, determined by Section 6.6. The model is a 9x9 package array of the GNF2 fuel bundle with lattice expansion to the inner container. Polyethylene in the model is a uniform wrap of the normal packing materials (i.e., cluster separator and sheathing bag) defined in Table 6-14. No ethafoam is represented; however the effect of packaging materials were evaluated in Appendix 6.9.6, and resulting effects are also taken into account for the polyethylene evaluation.

The largest positive reactivity from any polyethylene redistribution stage will be added as additional uncertainty to the total uncertainty due to modeling and geometric representations.

The volume of each melting material is calculated and then adjusted to conform to the calculated weighted packing material density of 0.947 g/cm^3. The two melting materials are the ethafoam cushioning and normal packing materials. The ethafoam represents a volume of 53189.6 cm^3 at the specification density of 0.08 g/cm^3, adjusting to the packing material density the volume becomes 4494.51 cm^3. The conversion is calculated by setting the masses of each model equal and solving for the volume at the adjusted density (e.g., $\rho_1 * V_1 = \rho_2 * V_2$, where V_2 is unknown). The normal packing materials is the combination of the sheathing bag and cluster separators, as defined in Table 6-14.

Volume, sheathing bag

$$Vbag = wbag * (Lfuel + 12" \; excess) * (2 * tbag)$$

Volume, cluster separator

$Vcs = (38LDPE + 85HDPE)cc * 2 * Nunits(32)$

Volume, packing = Volume, sheathing bag + Volume, cluster separator

$\rho_{packing} = (\rho cs * Vcs + \rho bag * Vbag)/Vpacking$

Volume, ethafoam = 53189.6 cm^3 at ρ=0.08 g/cm^3

At polyethylene weighted packing material density ρ=0.947g/cm^3 equivalent to V=4494.5 cm^3

Cases

1. Stage 1: normal, before melting model

Representing a normal condition of transport, prior to melting, Stage 1 is modeled with normal packing materials and ethafoam cushioning material in place. Additionally, the fuel bundle is modeled at the normal pitch without an expanded region. Cluster separators or inserts are placed into the assembly, between the rods at designated positions. For modeling, these pieces are assumed to be uniform polyethylene plates between each row of rods over the effective fuel length. The polyethylene plates are composed of the cluster separators and the sheathing bag, as the bag represents a small fraction of the volume and this modeling is simpler.

Separator plate thickness calculation:

An estimated total mass of the cluster separators is used to determine the plate thickness distributed over the length of the fuel between each row of rods in the assembly. Polyethylene materials properties are defined in Table 6-14, while assembly properties will be clearly defined in Section 1 (See RAI 6-1).

$$t_{plate} = \frac{M}{\rho \cdot N \cdot m \cdot p \cdot L}$$

where,

t_{plate} = polyethylene plate thickness

M = mass of packing

ρ = density of packing

N = # of rods

m = # of plates

p = pitch

L = active fuel length

2. Stage 2, ethafoam melt

The inner container ethafoam packaging materials are completely melted, hence material at the bottom side, four sides and upper side are accumulated at the bottom part of the inner container, whether the model is oriented vertically or horizontally. The ethafoam melted volume of 4494.5 cm^3 at 0.947 g/cm^3 is melted for stage 2. Due to melting of material, the fuel assemblies are moved downward and in contact with the bottom wall of the inner container. Therefore, the fully melted material fills part of the assembly and inner container evenly. Fuel rods are still covered with a uniform poly wrap composed of the packing materials, defined by Table 6-14.

For the horizontal model, fuel rods of the bottom row of the assembly are submerged in polyethylene, where the height of the polyethylene is defined by the nominal pitch of the assembly. However, for the expanded lattice the polyethylene fills the first row at the expanded lattice pitch. For simpler modeling, the addition of 2395 cm^3 of poly is added to the melt material to fully fill the bottom row of the assembly and create a uniform level in the IC the height of the first row of rods at the normal pitch.

For the vertical model, the poly melt height is calculated to match the volume of melted material to the nearest whole number. Hence a height of 22 cm is filled in with polyethylene, with the addition of 116 cm^3 of polyethylene for simpler modeling. The model is oriented with the expanded lattice at the bottom, so the polyethylene material fills in the expanded lattice region first.

3. Stage 3: full melt

With extended time, the materials are assumed to fully melt and accumulate at the bottom of the inner container, filling a potion of the assembly, uncovering the upper portion of the assembly from any polyethylene. Due to melting of material, the fuel assemblies are moved downward and in contact with the bottom wall of the inner container. Therefore, the fully melted material fills part of the assembly and inner container evenly. Stage 3 is represented by the assembly covered with melted ethafoam and normal packing materials with a combined total volume of 13056.3 cm^3 at weighted packing material density ρ=0.947 g/cm^3.

For the horizontal model, fuel rods of the bottom two rows of the assembly are submerged in polyethylene, where the height of the polyethylene is defined by the nominal pitch of the

assembly. However, for the expanded lattice the polyethylene fills two rows at the expanded lattice pitch. For simpler modeling, the addition of 456 cm^3 of poly is added to the melt material to fully fill two rows of the assembly and create a uniform level in the IC the height of two rows of rods at the normal pitch.

For the vertical model, the poly melt height is calculated to match the volume of melted material to the nearest whole number. Hence a height of 63 cm is filled in with polyethylene, with the addition of 146 cm^3 of polyethylene for simpler modeling. The model is oriented with the expanded lattice at the bottom, so the polyethylene material fills in the expanded lattice region first.

Table 6-Xa HAC, Polyethylene Redistribution Comparison

Analysis Condition	Analysis Model	Fuel Bundle		
		k_p	σ_p	Δk_p
HAC package array	Full wrap Horizontal / vertical	0.87473	0.00044	--
HAC package array (Intermediate state)	Stage 2: initial melt Horizontal	0.88072	0.00037	0.00585
HAC package array (Intermediate state)	Stage 2: initial melt Vertical	0.88610	0.00042	0.01133
HAC package array (Intermediate state)	Stage 3: full melt Horizontal	0.87410	0.00034	-0.00080
HAC package array (Intermediate state)	Stage 3: full melt Vertical	0.90206	0.00034	0.02713

Table 6-Xb NCT, Polyethylene Modeling Comparison

Analysis Condition	Analysis Model	Fuel Bundle		
		k_p	σ_p	Δk_p
NCT package array	Full wrap Horizontal / vertical	0.82792	0.00036	--
NCT package array	Stage 1: nominal – plates +ethafoam Horizontal / vertical	0.84605	0.00033	0.01807

RAI 6-35:

Revise Appendix 6.9.5 of the SAR to consider loose fuel rod designs within the proposed rod containers, or within the package inner container.

This appendix provides an infinite triangular pitch array evaluation of individual fuel rod designs to determine the most reactive type for inclusion in the loose rod criticality evaluation. This evaluation should be revised to consider rods within the package and rod container, as reflection conditions within the package and the mass of fissile material allowed by the assumed pitch, rod radius, and container envelope, may have a significant effect on calculated keff. Also note that this evaluation is performed assuming triangular pitch infinite array, whereas most of the evaluations within the package are modeled with a square pitch.

Response: (also see RAI 6-12 response)

The infinite fuel rod analysis uses the hexagonal lattice for comparison of fuel rod categories, as it allows more fuel within the specified rod spacing. The impact of the rod container effects are addressed in RAI 6-12, where various pitch types and spacing are evaluated per container. In addition to the selection of the most reactive fuel rod category (BWR_G3), the minimum (PWR_W5) and maximum (PWR_W3) fuel rod categories as based on fuel pellet diameter are evaluated for the fuel rod contents.

6.9.5 Fuel Rod Contents Evaluation

The fuel rod contents are evaluated by calculating an infinite *keff* for a range of fuel rod pitches that encompasses peak reactivity to determine a maximum reactivity. The fuel rod designs are categorized by cylindrical dimensions and evaluated based on category dimensions, as shown in Table 6-50. The longest fuel length of the fuel types per category is used to represent that particular fuel rod category. An optimum configuration of fuel rod pitch and diameter as determined by this evaluation is used in the package assessment for transport of fuel rods.

Table 6-50 Fuel Rod Parameters

Fuel Category	Fuel OR	Gap OR	Clad OR	Fuel Length	Fuel Types
BWR_W1	0.424	0.4315	0.492	390	SVEA
BWR_G1	0.478	0.4875	0.599	370.84	GE11, GE13
BWR_G2	0.438	0.447	0.513	405.5	GE12B, GE14C, GE14G
BWR_G3	0.444	0.453	0.513	381	GNF2
PWR_W1	0.4374	0.4463	0.508	365.76	14OFA
PWR_W2	0.4647	0.4742	0.5359	365.76	14STD, 15OFA
PWR_W3	0.4839	0.4928	0.5588	347.218	CE14
PWR_W4	0.4096	0.4178	0.475	381	16STD, CE16 NGF, 17STD
PWR_W5	0.3922	0.4001	0.4572	365.76	16NGF, 17OFA, VV6
PWR_W6	0.4128	0.4216	0.4851	381	CE16NVA
PWR_W7	0.4128	0.4216	0.4851	381	CE16VA, CE16

RAI 6-36:

Revise Appendix 6.9.6 of the SAR to clarify whether the effect of packaging materials is evaluated considering fuel assemblies with or without BA rods.

This appendix provides an evaluation of the effect of packaging materials on calculated keff but does not state whether this evaluation is performed with or without BA rods in the assembly. This evaluation parameter would be expected to have an effect on the results of the analysis, and as such should be clarified and justified in the description.

Response:

Text updates to subsections of 6.9.6, as shown below, are for clarification of the fuels used to evaluate the effect of packaging materials.

6.9.6 Effect of Packaging Materials

The effect of packaging materials is evaluated by calculating the effect that the material has on k_p relative to a reference configuration as follows:

Individual package	Water in all void space and water in regions normally filled with thermal insulator, foam cushion, and impact limiter. Establishes a reference value for k_{eff} that maximizes neutron reflection for the confinement system.
Package array	Void in regions normally filled with thermal insulator, foam cushion, and impact limiter. Water filled in the fuel region. Establish a reference value for k_{eff} for neutron interaction between packages....

6.9.6.1 Individual Package

The effect of the packaging material for an individual package is evaluated using GE14C and SVEA fuel bundle contents without BA rods as this allows the most flexibility for shipment of an individual package. Figures 6-36 and 6-37 show the effects of the packaging materials on an individual package for the following packaging material configurations:

...

6.9.6.2 Package Array

The effect of the packaging material for the package array is evaluated using a GNF2 and SVEA fuel bundle contents with BA rods, as this represents the most common configuration for

shipment of a package array. Figures 6-38 and 6-39 show the effects of the packaging materials on a package array for the following packaging material configurations:

...

RAI 6-37:

Revise Section 6.9.6.2 of Appendix 6.9 to clarify the modeling assumptions for the packaging array package material effects.

The text of this section states that package array is evaluated with void in significant portions of the model, while Table 6-53 shows that these same portions are evaluated with water. The table and related text should be revised to clarify this issue.

Response:

Text is correct, as the package array analysis is modeled with void as the base case and the individual package analysis is modeled with water as the base case; therefore Table 6-53, Figure 6-40, and Figure 6-41 updated as follows:

Table 6-53 Packaging Material Effects, Package Array

Fuel Type	Packaging Configuration	Confinement Boundary			
		Nominal	Fuel Channel	Inner Container	
	Material (Region)	Δk_p	Δk_p	Δk_p	Δk_p *Average*
GNF2					
	AlSi (1) Void (2,4)	-0.00327	-0.00332	-0.00320	-0.00326
	Poly (2), Void (1,4)	-0.01314	-0.01346	-0.01601	-0.01420
	Pack Material (3), Void (1,2,4)	0.00324	0.00292	0.00221	0.00279
	Char (4), Void (1,2)	-0.00725	-0.00676	-0.00642	-0.00681
SVEA					
	AlSi (1) Void (2,4)	-0.00270	-0.00328	-0.00264	-0.00287
	Poly (2), Void (1,4)	-0.00812	-0.00909	-0.01003	-0.00908
	Pack Material (3), Void (1,2,4)	0.00396	0.00335	0.00231	0.00321
	Char (4), Void (1,2)	-0.00545	-0.00634	-0.00628	-0.00602
AVERAGE for SVEA and GNF2					
	AlSi (1) Void (2,4)	-0.00135	-0.00164	-0.00132	-0.00144
	Poly (2), Void (1,4)	-0.00570	-0.0062	-0.00662	-0.00617
	Pack Material (3), Void (1,2,4)	0.00360	0.00314	0.00226	0.00300
	Char (4), Void (1,2)	-0.00110	-0.00171	-0.00204	-0.00162

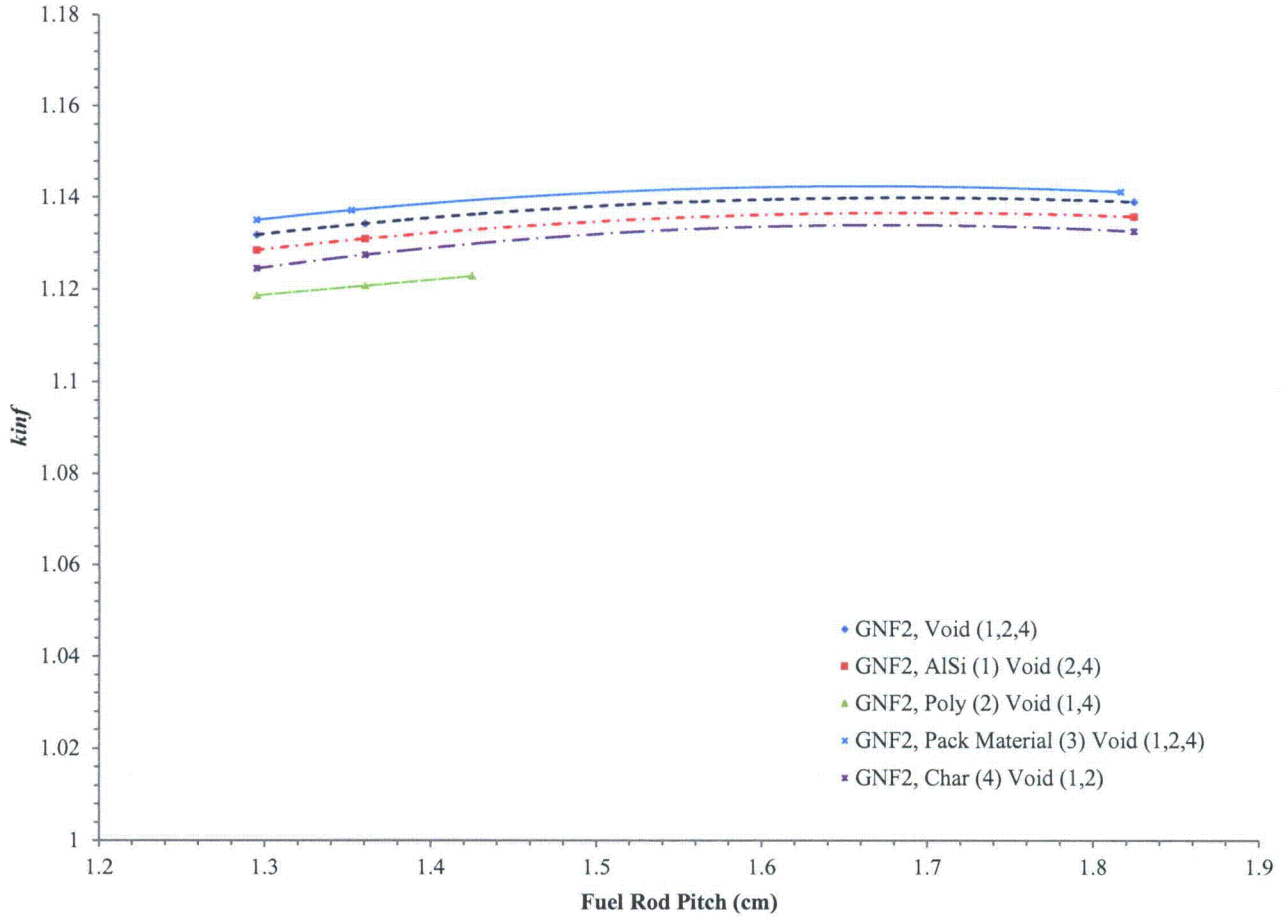

Packaging Configuration	Confinement Boundary					
	Nominal		Fuel Channel		Inner Container	
Material (Region)	k_p	σ_p	k_p	σ_p	k_p	σ_p
Void (1,2,4)	1.13173	0.00028	1.13417	0.00026	1.13883	0.00026
AlSi (1) Void (2,4)	1.12846	0.0003	1.13085	0.00025	1.13563	0.0003
Poly (2), Void (1,4)	1.11859	0.00026	1.12071	0.0003	1.12282	0.00032
Pack Material (3), Void (1,2,4)	1.13497	0.0003	1.13709	0.00025	1.14104	0.0003
Char (4), Void (1,2)	1.12448	0.00029	1.12741	0.00031	1.13241	0.00028

Figure Error! No text of specified style in document.**-40 Packaging Material Effect, Package Array (Infinite), GNF2**

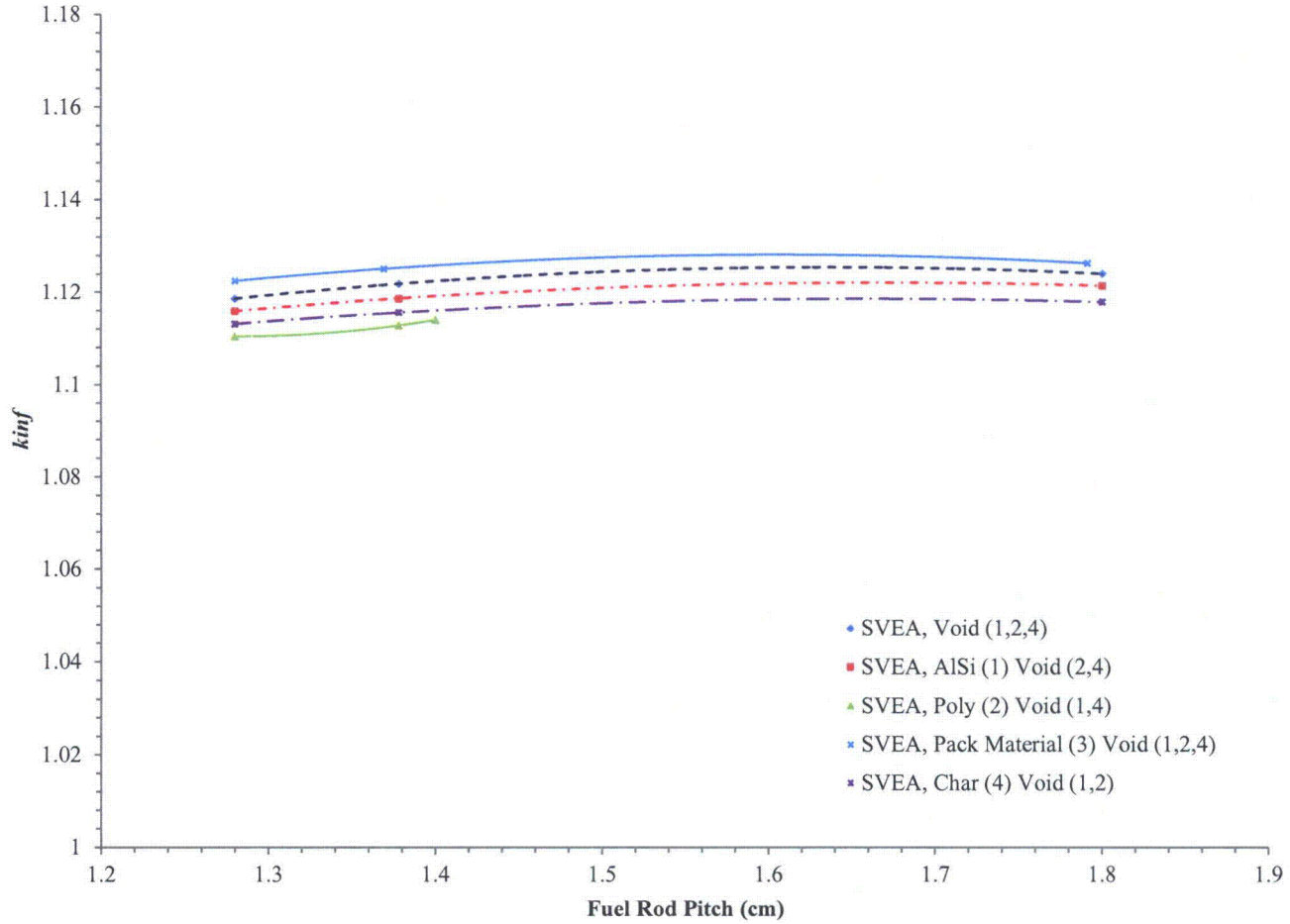

Packaging Configuration	Confinement Boundary					
	Nominal		Fuel Channel		Inner Container	
Material (Region)	k_p	σ_p	k_p	σ_p	k_p	σ_p
Void (1,2,3,4)	1.1185	0.00029	1.12180	0.00028	1.12392	0.00027
AlSi (1) Void (2,3,4)	1.11580	0.00027	1.11852	0.00025	1.12128	0.00026
Poly (2), Void (1,3,4)	1.11038	0.00026	1.11271	0.0003	1.11389	0.00026
Pack Material (3), Void (1,2,4)	1.12246	0.00035	1.12515	0.00028	1.12623	0.00029
Char (4), Void (1,2,3)	1.11305	0.00029	1.11546	0.00027	1.11764	0.00029

Figure 6-41 Packaging Material Effect, Package Array (Infinite), SVEA